Inundation and evacuation of shoreline populations during landslide-triggered tsunami: An integrated numerical and statistical hazard assessment

Emmie M. Bonilauri[1], Catherine Aaron[2], Matteo Cerminara[3], Raphaël Paris[1], Tomaso Esposti Ongaro[3],
5 Benedetta Calusi[3,4], Domenico Mangione[5] and Andrew J.L. Harris[1]

[1]Laboratoire Magmas et Volcans, OPGC, IRD, CNRS, Université Clermont Auvergne, Clermont – Ferrand, 63170, France
[2]Laboratoire de Mathématiques Blaise Pascal, CNRS, Université Clermont Auvergne, Clermont – Ferrand, 63170, France
[3]Istituto Nazionale di Geofisica e Vulcanologia (INGV), Sezione di Pisa, Pisa, 56125, Italy
[4]Dipartimento di Matematica e Informatica Ulisse Dini, Università degli Studi di Firenze, Firenze, 50134, Italy
10 [5]Dipartimento della Protezione Civile, Rome, 00189, Italy

Correspondence to: Emmie M. Bonilauri (Emmie.BONILAURI@uca.fr, emmie.bonilauri@gmail.com)

Abstract. The volcanic island of Stromboli (Southern Tyrrhenian sea, Italy) is renowned for its persistent, periodic, low-intensity explosive activity, whose spectacular manifestations attract tens of thousands of tourists every year. However, sporadic more intense major explosive and effusive eruptions, and paroxysms, pose serious threats to the island. In addition

15 to direct hazards, granular slides of volcanic debris and pyroclastic avalanches, which can rapidly reach the sea potentially generating tsunamis, are often associated with such unpredictable eruptive activity. Due to the very fast propagation of the tsunami around the island, and the consequent short tsunami warning time (ranging from less than a minute to only a few minutes) mitigation efforts and evacuation from the Strombolian coast must be carefully planned. In this paper, we describe a new, GIS-assisted procedure that allows us to combine the outputs of an ensemble of 156 pre-computed landslide-

20 generated tsunami hazard scenarios (with variable landslide volume, position, and density), statistical exposure data (i.e., the number of inhabitants and tourists) and digital geographic information, to obtain a quantitative (scenario-based) risk analysis. By means of the analysis of the road network and coastal morphology, we develop a model with routes and times to reach a safe area from every pixel in the inundated area, and appraisal for the time needed to escape versus the wave arrival time. This allows us to evaluate and quantify the effectiveness of potential risk mitigation by means of evacuation. The

25 creation of an impact score linking the predicted inundation extent and the tsunami warning signals is intended, in the long term, to predict the intensity of future tsunamis, and to adapt evacuation plans accordingly. The model, here applied to Stromboli, is general, and can be applied to other volcanic islands. Evacuating an island hosting several thousand tourists every summer with very little warning time supports the absolute necessity for such mitigation efforts, aimed at informing hazard planners and managers, and all other stakeholders.

1 Introduction

The NOAA's NCEI (National Center for Environmental Information) estimates that about 81% of recorded tsunamis originate from earthquakes, with 7% originating from landslides and 5% from volcanoes, the remaining 5% being from an unknown source (NCEI; Harbitz et al., 2014). Landslide-generated tsunamis vary greatly in their size and origin, with volcano flank collapse being a frequent source. The range of volume and position of the collapse on the volcano flank produces great variation in terms of coastal impact (Grezio et al., 2017). Large volume collapse of flank of a volcano island can, for example, generate local tsunamis with waves tens of metres high in the proximal fields (Paris et al., 2018). However, tsunamis caused by volcanic landslides are characterized by shorter wavelengths compared to earthquake-induced tsunamis (Grezio et al., 2017), and consequently their far-field effect is often considerably reduced compared to their proximal impact as observed, e.g., during the 2018 Anak Krakatau tsunami (Muhari et al., 2019). However, even a 1 m high tsunami inundating a beach can present a high risk to populated coastlines and tourist seaside resorts.

At Stromboli, an active volcano of the Aeolian archipelago (Southern Tyrrhenian sea, Italy; Rosi et al., 2000, 2013) tsunamis can be potentially generated by instability and collapse of volcano flanks (in particular, the steep north-western slope of the Sciara del Fuoco) or by pyroclastic currents generated by paroxysmal eruptions (Pistolesi et al., 2020; Giordano and De Astis, 2020). One example of a tsunami generated by a landslide is that of Stromboli in December 2002. In that case, two landslides generated two tsunamis 7 minutes apart with maximum run-up of 10.9 m (Tinti et al., 2006a). The first tsunami was due to a near-shore submarine landslide, probably involving up to 20×10^6 m^3 of material (Chiocci et al., 2003), and the second by a subaerial landslide of $4 - 9 \times 10^6$ m^3 that broke off at about 500 m a.s.l (Tinti et al., 2006b). The resulting tsunami caused significant damage along the island coast up to an elevation of about 10 m above sea-level (Tinti et al., 2006a; Fornaciai et al., 2022), as well as at the island of Panarea 21 km distant (Maramai et al., 2005a).

The risk associated with tsunamis is particularly high on Stromboli, due the high density of population on the coasts, and where travel time for the tsunami from the source is minutes (Bonilauri et al., 2021). This is enhanced at Stromboli where, with the development of global tourism, vacation rentals, restaurants, shops, and hotels have been built close to the beaches. With the development of tourism and influx of seasonal workers, the collective memory linked to the tsunami risk also becomes reduced (Tulius, 2020; Riskianingrum and Yogaswara, 2022).

For these reasons, after the 2002 events, the scientific community and the Italian Civil Protection Department undertook a series of initiatives aimed at quantifying the hazards associated with landslide-generated tsunamis, providing an early detection and alert system, to mitigate the associated risks. In particular, the Laboratorio di Geofisica Sperimentale (LGS) of the University of Florence installed two tsunami detection beacons: the first in 2008 at the South-West of the foot of the Sciara del Fuoco and the second in 2017 at the North-East (Selva et al., 2021). To be able to generate an automatic alert and warn the relevant authorities and the population as quickly as possible, they have developed a tsunami detection algorithm by studying the STA/LTA (Short Time Average over Long Time Average) ratio and the dispersion of surface waves (Lacanna and Ripepe, 2020; Selva et al., 2021). They were able to test the algorithm successfully during the two paroxysms

in July and August 2019 (Lacanna and Ripepe, 2020; Selva et al., 2021) and during the avalanche caused by the partial collapse of the NE crater on the 4th of December of 2022.

65   In parallel, a systematic study has been carried out to define tsunami hazard scenarios based on several, complementary approaches. The first is the identification of past events in the sedimentological record (tsunami deposits) and historical archives in order to build a tsunami catalogue (Maramai et al., 2014; Pistolesi et al., 2020). The second is based on the interpretation of observations and instrumental data (Bonaccorso et al., 2003; Pino et al., 2004; Boldini et al., 2005; Calvari et al., 2005; Maramai et al., 2005a,b; Tinti et al., 2005; Tommasi et al., 2005; Acocella et al., 2006; Tinti et al., 2006a,b;

70   Chiocci et al., 2008a,b; Fornaciai et al., 2022). The third comprises model-based scenarios through data-driven simulations (Fornaciai et al., 2019; Bonilauri et al., 2021; Esposti Ongaro et al., 2021).

Finally, a series of initiatives have been carried out to enhance the awareness about the tsunami risk and to enforce mitigation actions aimed at the timely evacuation of the risk zones in case of tsunami via the "Io non rischio" awareness campaign (https://www.iononrischio.gov.it/en/get-ready/volcanoes/stromboli/what-do/) and by several work tasks as the

75   ongoing Task 4.3 of DPC-INGV 2022-2024 Agreement for the implementation of the service activities: "Survey on risk perception of explosive paroxysms and tsunamis to better define a communication strategy and informative materials".

In this paper, we describe a new procedure that allows us to combine the outputs of an ensemble of pre-computed tsunami hazard scenarios and exposure data and digital geographic information, to obtain a quantitative (scenario-based) risk analysis and to quantify the effectiveness of potential risk mitigation by means of evacuation. In our procedure, the tsunami hazard is

80   represented by a set of (static, georeferenced raster) maps of inundation (maximum wave height above ground) and wave arrival times, one for every individual scenario produced by numerical simulations. Every tsunami scenario is in turn defined, in a deterministic approach, by a corresponding landslide scenario, and it is associated with a trigger time (which approximately corresponds to the initial time at which an alert is issued). For every scenario, we are able to calculate an "impact score", which classifies in a simple and intuitive way the scenarios in terms of their impact on the island shores. For

85   exposure, we consider the population distribution on the island and the geometry of the road network, with which we can compute escape times from any pixel of the map towards a Refuge Area Entry Point (RAEP). By convolving hazard and exposure maps, we are then able to obtain maps expressing the level of risk of the different areas along the Stromboli shores, in terms of potential impact of a given scenario and potential mitigation in terms of evacuation capacity.

The procedure here applied to the island of Stromboli is a general one, and we discuss in the following sections its main

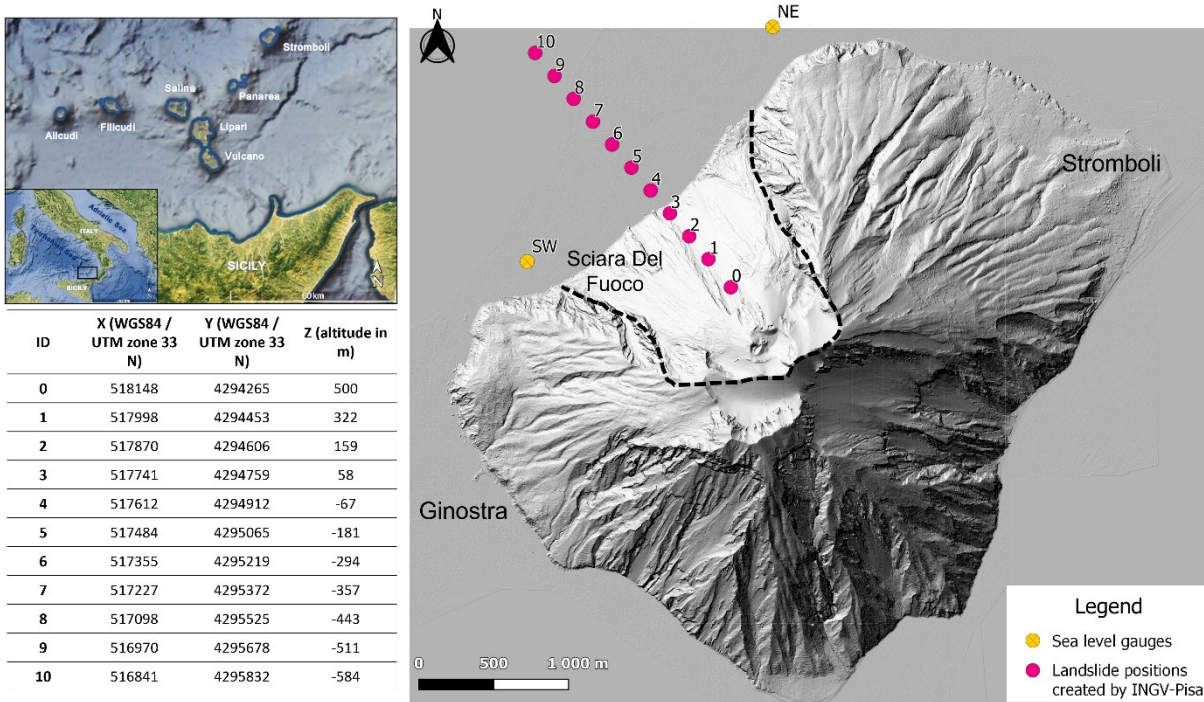90   components, assumptions, and criticalities.

2 Methods

2.1 Tsunami hazard scenarios

In this paper, we base our analysis on tsunami scenarios produced by numerical simulations with a coupled landslide-water multilayer, non-hydrostatic shallow water model (Esposti Ongaro et al., 2021). The landslide is considered as a granular

95   fluid, having a given initial volume, position, and density, which is dynamically two-way coupled with the water layers. The Multilayer-HySEA (Hyperbolic Systems and Efficient Algorithms) numerical model (Fernández-Nieto et al., 2018; Macías et al., 2021a,b) adopted to generated the scenarios is particularly suited to the case of a volcanic island, since typical landslide-generated tsunamis have short wavelengths and develop over steep topo-bathymetry, making the usual hydrostatic approximation fail.

100 Simulations using Multilayer-HySEA were performed using ten different initial landslide positions (positions 1 to 10, Figure 1), five different volumes (5, 8, 14, 21, and 30×10^6 m^3) and three different densities (2.5, 2.0 and 1.7 kg/m^3, or water/landslide density contrasts of 0.4, 0.5, 0.6, respectively), basing on the ranges hypothesized for the 2002 tsunami event at Stromboli (Fornaciai et al., 2019; Esposti Ongaro et al., 2021). Additional simulations from a higher subaerial position (Position 0, Figure 1) were run with two different volumes, for a total of 156 simulations analysed. For each simulation, we

105 consider (1) the coastal inundation (i.e., the estimated inundation depth for each onshore pixel); (2) the tsunami arrival time for each pixel in the inundated area; (3) the offshore water surface elevation.

ID	X (WGS84 / UTM zone 33 N)	Y (WGS84 / UTM zone 33 N)	Z (altitude in m)
0	518148	4294265	500
1	517998	4294453	322
2	517870	4294606	159
3	517741	4294759	58
4	517612	4294912	-67
5	517484	4295065	-181
6	517355	4295219	-294
7	517227	4295372	-357
8	517098	4295525	-443
9	516970	4295678	-511
10	516841	4295832	-584

Figure 1: Location of Stromboli Island and landslide position numbers simulated by the INGV of Pisa with their respective coordinates and altitudes, position number 0 corresponding to December 2002 characteristics. The authors made maps by using
110 **Quantum GIS version 3.16.7 software (2021).**

For each simulation, we also define an onset time T_0, when the landslide starts, a final time T_{600}, when the simulation is stopped, and "trigger time" T_g, when the generated wave overcomes a given threshold at one of the two gauges offshore the Sciara del Fuoco. These are located on the position of the actual beacons, installed close to Punta Labronzo (North East Beacon, BNE) and Punta dei Corvi (SouthWest Beacon, BSW). In this work, we decided to adopt a threshold of +0.3 m or -

115 0.3 m on the wave detection at the gauges, to analyse only "significant" scenarios in terms of impact. The choice of such a threshold was done on a subjective basis and might be the object of further analysis in the future.

The trigger time T_g should be approximatively equivalent to the time at which the alert is issued, following the procedure described by Selva et al (2021) and Lacanna and Ripepe (2020). Finally, the wave arrival time at a given pixel is computed as the difference between the actual tsunami arrival time and the trigger time T_g.

120 All simulation and post-processed data were integrated in QGIS (Quantum GIS) 3.16.7 with GRASS (Geographic Resources Analysis Support System) version 7.8.5. Topography was represented by a Digital Elevation Model (DEM) of 31635 pixels (20 m by 20 m) from the LiDAR (Light Detection And Ranging) campaign carried out in July 2010 by the INGV and bathymetry was from the Marine Geohazards along the Italian Coasts (MaGIC) project (for more details, see: Favalli et al., 2009; Chiocci and Ridente, 2011; Fornaciai et al., 2019).

2.2 Inundation Impact Score and link with the proximal wave height

For each landslide and tsunami scenario, we define an "impact score" S, equal to the number of on land pixels (in the digital model) that are inundated at a given time, during the numerical simulation (we might also consider our impact score in terms of inundated area in m²). The impact score allows us to classify the landslide-tsunami scenarios based on their coastal hazard and to link such a hazard to the features of the tsunami at the proximal gauge. In particular, we have used several statistical methods to try to establish a robust link between the impact score and the maximum wave height at the proximal gauge, which is, in principle, a measurable quantity. The statistical procedure is described in detail in Appendix A.

2.3 Pedestrian horizontal evacuation model

For every simulated scenario, we applied an evacuation model to each inundated pixel, by using the approach of Bonilauri et al. (2021). This is a macroscopic model, i.e., a model for global evacuation and not an agent-based approach, which determines the fastest pedestrian evacuation paths from a danger point to a safe point, and compares the escape time with the wave arrival time.

To apply the evacuation model, a grid with the same mesh size as the inundation model (20 m) was created for the village of Stromboli (Figure 2), and a centroid, i.e., an evacuation starting point, was placed central to each pixel. A speed reduction coefficient was assigned to each road segment according to its width, slope, and surface type (Table 1). For each tsunami simulation, the quickest escape routes were projected from each inundated centroid, and times required to evacuate each inundated pixel were calculated; with evacuation time being the time needed to move from the inundated pixel to a "safe" zone defined by the limit of the area impacted by the tsunami.

To reach the safe zone, evacuees must pass through a Refuge Area Entry Points (RAEP). Two categories of RAEP were established:

145   1. A *normal-event* RAEP was assigned for tsunamis with run-ups less than or approximately equal to that of the December 2002 event, i.e., the RAEP was placed at the intersection between road network and 15 m contour line.

2. An *extreme-event* RAEP was set for tsunamis greater than the December 2002 run-up, and placed at the intersection between road network and 35–40 m contour line.

150   **Figure 2: Establishment of baseline data: starting centroids for the numerical simulation of a 30 million m^3 tsunamigenic landslide that detached from position number 6 (294 m below sea level) with a density of volcanic materials of 2.5 kg/m^3, Stromboli road network and Refuge Area Entry Point, to run evacuation models. Map was produced by the authors using Quantum GIS version 3.16.7 software (2021).**

Table 1: Pedestrian evacuation speeds depending on land slope and road types (Péroche, 2016; Bonilauri et al., 2021)

Class	Slope value (%)	Associated speed (km/h)	Speeds after application of reduction coefficient (km/h)		
			Two-lane road	Single-lane road	Passageway, path, stairs, unsurfaced track
Reduction coefficient			1	0.8	0.5
1	< 3	4.85	4.85	3.88	2.43
2	[3–6[	4.55	4.55	3.64	2.28
3	[6–9[	4.26	4.26	3.41	2.13
4	[9–12[	3.97	3.97	3.18	1.99
5	[12–15[	3.69	3.69	2.95	1.85
6	[15–18[	3.42	3.42	2.74	1.71
7	[18–21[	3.15	3.15	2.52	1.58
8	[21–24[	2.90	2.90	2.32	1.45
9	[24–27[	2.65	2.65	2.12	1.33
10	≥ 27	1.71	1.71	1.37	0.86

For each inundated pixel the difference between the time needed for escape and the wave travel time to the pixel was calculated. In particular, we used two source-to-pixel travel times. Firstly, we used T_0, i.e., the onset time of the landslide trigger, then T_g, the time of first detection of the generated tsunami at one of the two beacons. It is worth highlighting that the use of T_0 gives a longer escape time, but using T_g is more realistic given the current beacon-based alert system.

Finally, a spatial population distribution layer (Figure 3) was created using publicly available data, allowing the creation of three categories of population:

- Population in accommodation, i.e., resident in holiday rentals, hotels and bed & breakfast (B&B) locations. Capacities for all active establishments were taken from Booking.com, Airbnb, Tripadvisor, Vrbo, Abritel, Gites.fr and Cybevasion.fr, as well as individual rental/hotel/B&B websites.

- Populations using restaurants, bars, and cafes, with capacities assessed from Tripadvisor and Google images.

- Pedestrian traffic in and out of the port and visitors to beaches. These were taken from our own pictures and head counts made during surveys in September 2022, and in June and September 2023.
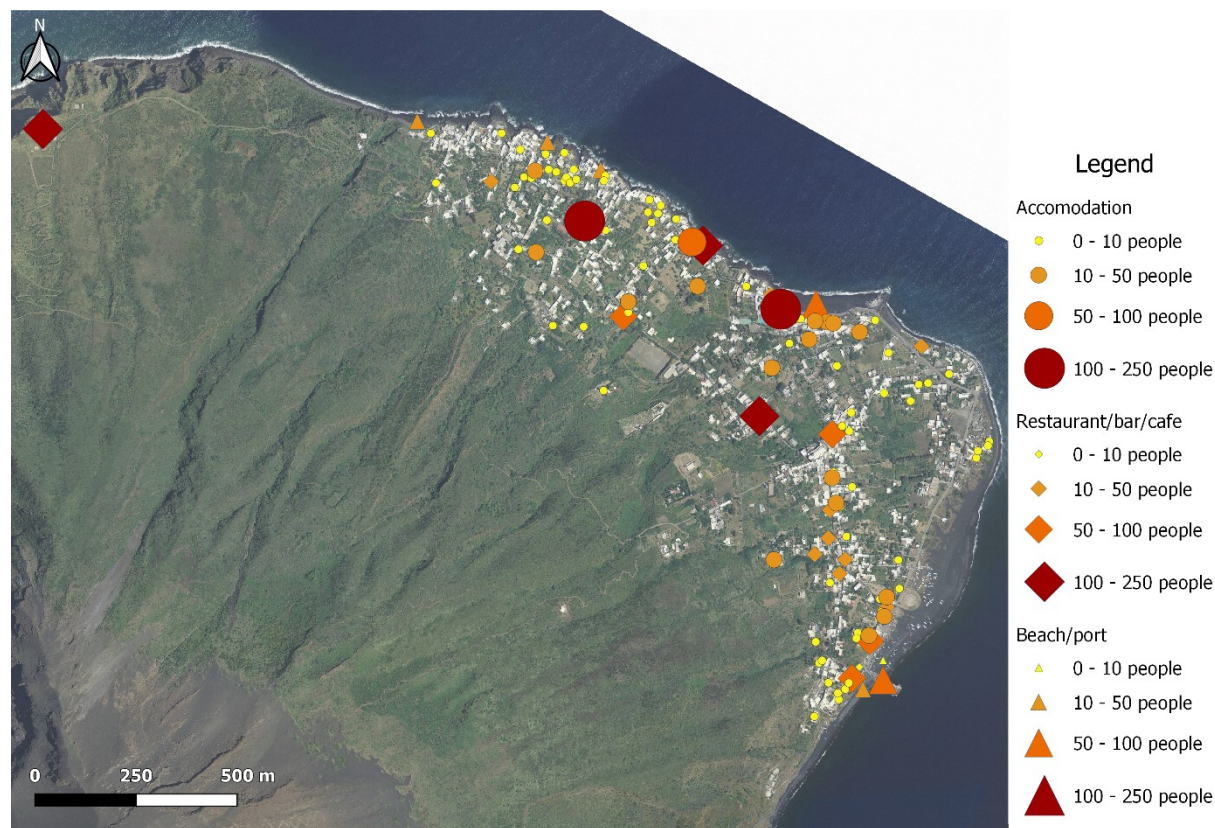
Figure 3: Spatial distribution of population on Stromboli Island based on Internet public data (accommodation, restaurant/bar/cafe, and beach/port). The authors produced maps by using Quantum GIS version 3.16.7 software (2021).

For locations where information was not available, we averaged the available capacity of the holiday rentals found and used a density of one person per 12.3 square metres. We then determined occupation scenarios by season and time of day. This distinguished between winter, when only the permanent population (≤150) is present, and the summer tourist season when as many as 5000 visitors can be on the island. It also distinguished between morning, midday, afternoon, evening, and night between which the distribution of workers and tourists between accommodation, restaurants-bars-cafes, and beaches/port varies.

Combining the vulnerability determined from these surveys with the hazard output for each of the 156 tsunami simulations provided the number of pixels inundated plus, for each inundated pixel:

- wave arrival time (T_{arrive}), where T_{arrive} is the moment when the generated tsunami has reached a pixel and inundation begins to be detected (1 cm threshold). T_{arrive} is calculated from T_g;

- inundation depth (i.e., water thickness above ground level);

8

- evacuation time (T_{evac}), where T_{evac} is the moment when evacuees reach a Refuge Area Entry Points (RAEP);

- "evacuability" (= T_{arrive} - T_{evac});

- number of people in need of evacuation.

185 We statistically convolved these metrics to allow a full and robust, scenario-based risk assessment, which includes generation of probability of inundation and impact score.

3 Results

3.1 Analysis of individual scenarios: arrival time and coastal impact

The simulation outputs range from tsunamis of just 0.22 m in amplitude, with a run-up of 0.29 m and impacting only some
190 parts of the beaches, to tsunamis with amplitudes of 48.1 m and run-ups of 24.2 m that inundate almost the entire village. For means of demonstration, we take a mid-range example that falls between these two extremes. This involves scenario-P6V30CD0.4, the simulation of a submarine landslide involving 30×10^6 m³ of volcanic material with a density of 2.5 kg/m³ from position number 6 (centred at 294 m below sea level). The generated tsunami inundates an area of 544 pixels, i.e., a surface of approximately 217 600 m², with the wave trapped around the entire island (Figure 4a). Refraction of the wave
195 causes some variation in tsunami travel times over short distances, where arrival times (computed using the trigger time T_0 as an initial time) vary from 48 s at Spiaggia Lunga (north of Piscità), to 154 s at Ficogrande, and 188 s and 242 s at Punta Lena and the port at Scari, respectively (Figure 4b). These four vulnerable sites are distant from the Sciara del Fuoco by about 2.4, 3.5, 4.1 and 4.9 km, respectively. The arrival times computed using the landslide onset time T_0 as an initial time are 20 s longer.
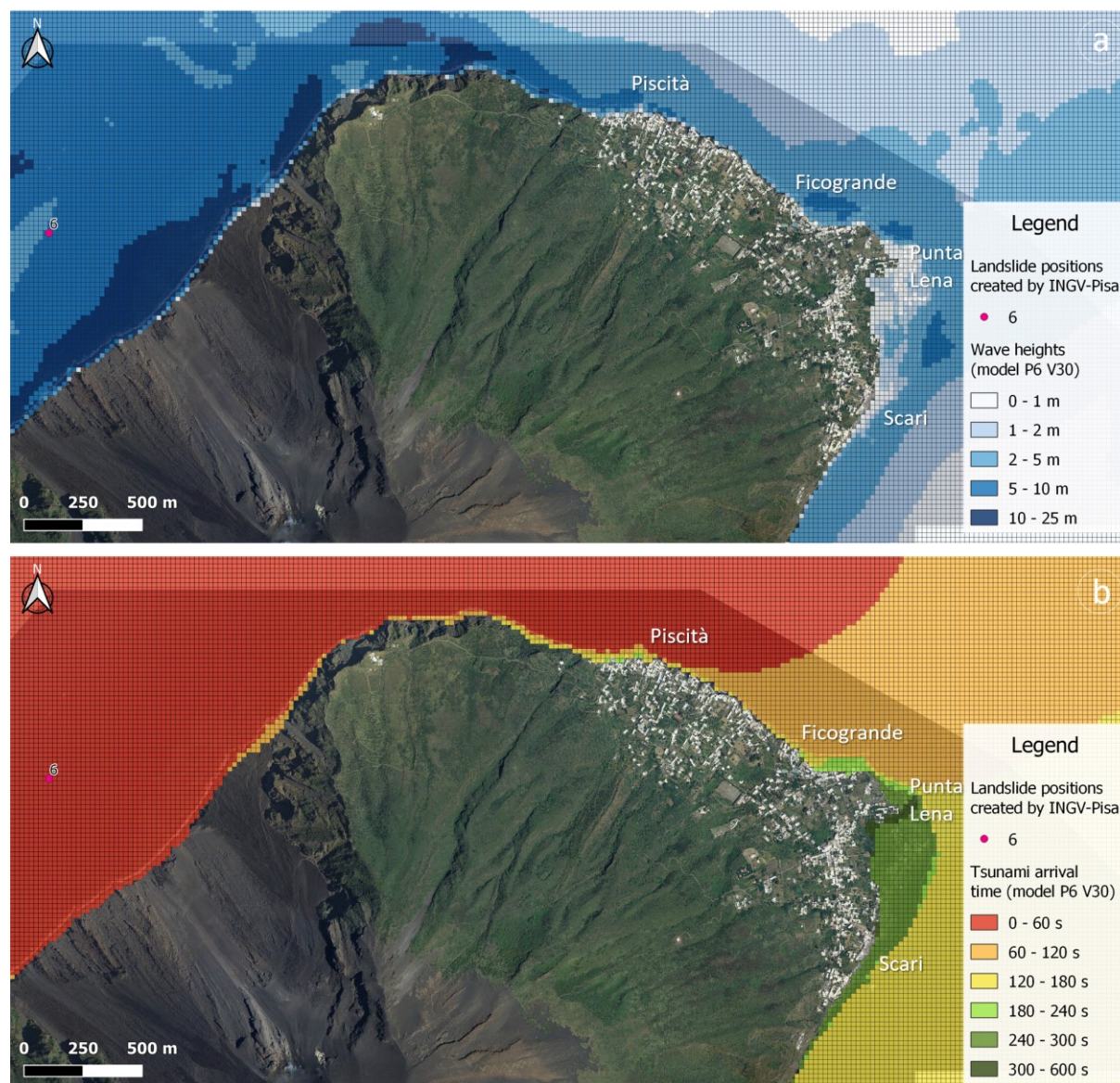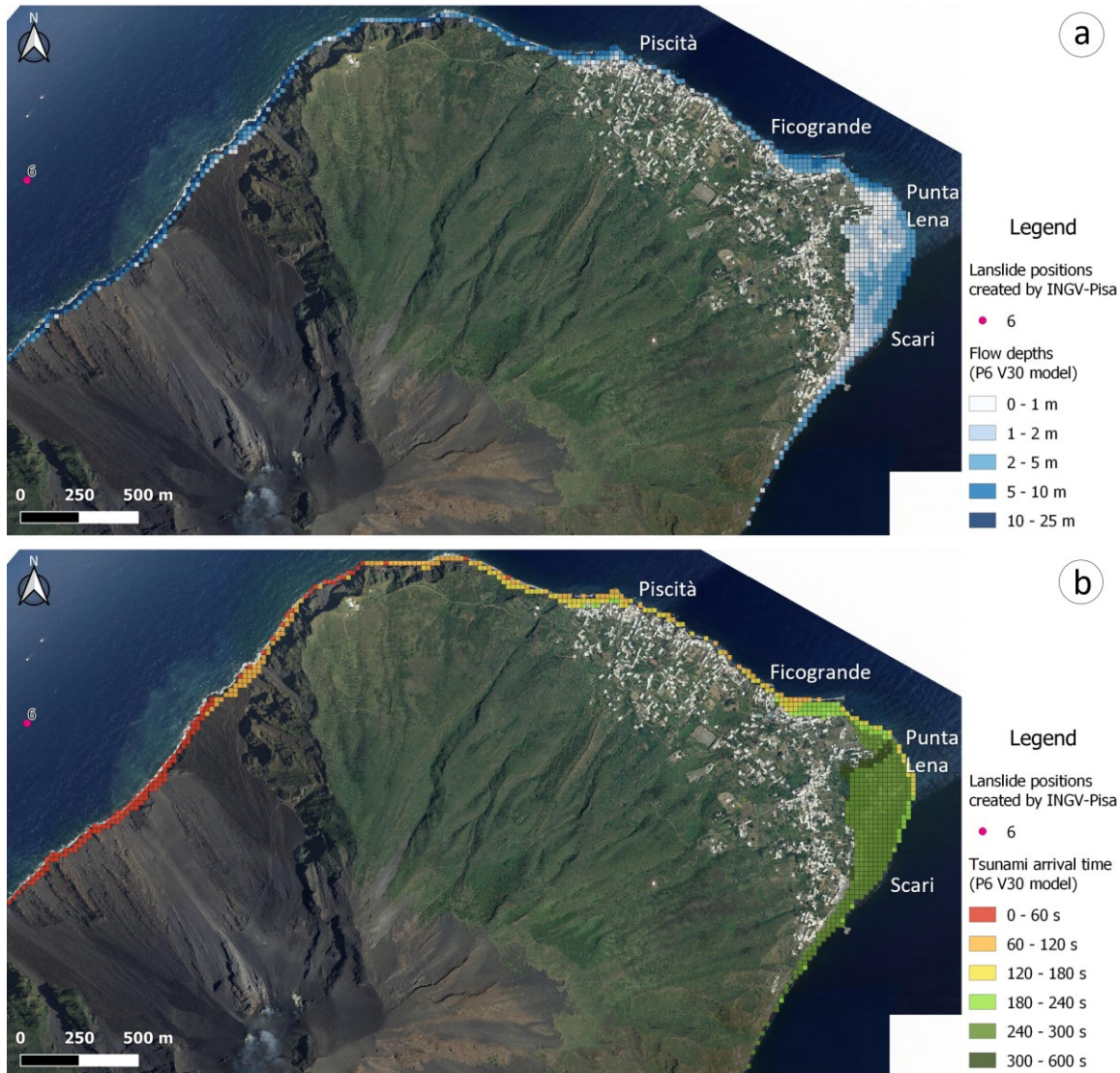
Figure 4: Example of a numerical simulation for a 30 million m3 tsunamigenic landslide that detached from position number 6 (294 m below sea level) with a density of volcanic materials of 2.5 kg/m3. a) Sea level variation around the island of Stromboli due to the propagation of the tsunami wave. b) Time of travel of the tsunami wave around Stromboli. The authors produced maps by using Quantum GIS version 3.16.7 software (2021).

The coastal inundation simulation for scenario-P6V30CD0.4, i.e., the maximum height above ground of water reached by the tsunami in each inundated pixel, is represented in Figure 5a. Inundation depths are highly variable due to the topography of the village which is underlain by around 11 lava flow fields, erupted from eccentric vents just above the village, between 15 and 2 ka (Calvari et al., 2011; Speranza et al., 2008). To the north of the village while the Spiaggia Lunga is well-exposed, the 20–30 m-high sea cliffs behind it protect the road and building behind it from inundation. The same is true for

10

210 Piscità, the first district of Stromboli to be reached by the tsunami, which is protected due to its location on the San Bartolo lava flow field. The same presence of the lava flow field along a coastal length of 1 km means that 10 m high cliffs protect the population as far as Ficogrande. Instead, Ficogrande is a bay located at the SE edge of the San Bartolo lava flow field, which focuses the tsunami wave and produces an increase in run-up behind the bay. To the SE of Ficogrande another 0.2 km stretch of coast is protected by the 15m high sea cliffs associated with the San Vincenzo lava flow field. However, beyond

215 this in the southern part of Punta Lena and the northern part of Scari the coastal topography relatively flat coastal for an area extending up to 150-200 m inland, resulting in an increase in the extent of inundation. Refraction of the tsunami wave around the island produces a decrease in the wave height to the south, causing low levels of inundation south of Scari.

The peculiar behaviour of wave propagation around the island impacts the arrival times of tsunamis too. This is particularly true in the low promontory of Punta Lena. Here we observe a narrow, in-land extending band of pixels on the north side of

220 the promontory with an arrival time of 300–600 seconds, while pixels immediately to the south have an arrival time between 120 and 300 seconds (Figure 5b).

Figure 5: Example of a numerical simulation for a 30 million m^3 tsunamigenic landslide that detached from position 6 (294 m below sea level) with a density of volcanic materials of 2.5 kg/m^3. a/ Extent of inundation zone and flow depths. b/ Arrival time of the landslide-induced tsunami on Stromboli coasts. The authors produced maps by using Quantum GIS version 3.16.7 software (2021).
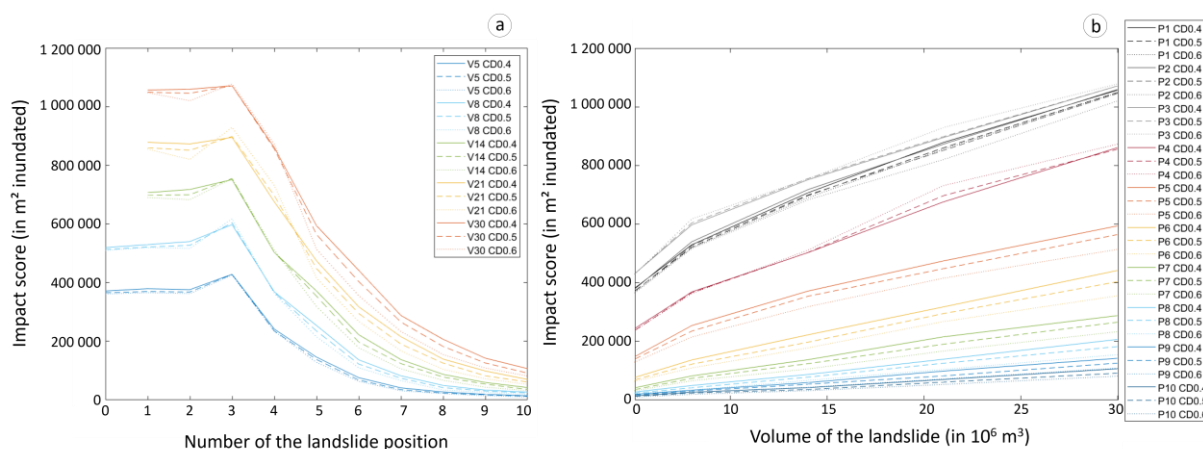
3.2 Impact score

Figure 6 shows the impact score function of landslide position and volume. After no change in the score between positions 0 and 3, the impact score systematically decreases as a function of landslide position between locations 4 and 10 (Figure 6a). The level of impact increases with volume, but with each curve having a similar shape. Subaerial positions (i.e., position numbers 0–3, Figure 1) have higher impact levels, but with little dependence on altitude. In the case of submarine positions (i.e., position numbers 4–10, Figure 1), there impact decreases with depth (below sea level) of the landslide source. For all

positions there is a positive, and broadly linear, relation impact and volume (Figure 6b). In the case of the subaerial positions, position 3 which is closest to sea level (Figure 1), shows a slightly higher impact score than the higher elevation subaerial positions 0, 1 and 2. This effect is related to the fact that the sliding volume of volcanic material has not had time to deform before reaching the sea surface, so that its entry is more focused.


Figure 6: Evolution of the impact score as a function of a/ position for each volume of volcanic material landslide in the Sciara del Fuoco and as a function of b/ volume for each landslide position (Position 0 to Position 3: subaerial landslide; Position 4 to Position 10: submarine landslide). The authors produced graphs by using MATLAB version 2019b.

3.3 Analysis of the signals at virtual gauges and link with the impact score

In Figure 7, we link the impact score for each scenario to the absolute value of the wave height. It is worth noting that in the evacuation analysis we used an initial time defined by T_g, i.e., the moment when a signal with an amplitude higher than a threshold of 0.3 m is detected. Please note that in the cases in which the signal never reaches this threshold, we assume that the landslide will not generate a tsunami large enough to require an evacuation and will therefore not be considered. Figure 8 shows the wave heights registered at the NE gauge (Figure 7a) and the SW gauge (Figure 7b) in the first 40 s (starting from T_0). The first peak is in most cases detected between 20 and 28 s at the NE beacon and between 8 and 16 seconds at the SW beacon. Not surprisingly, we observe that the highest impact scores are always associated with the highest wave heights.
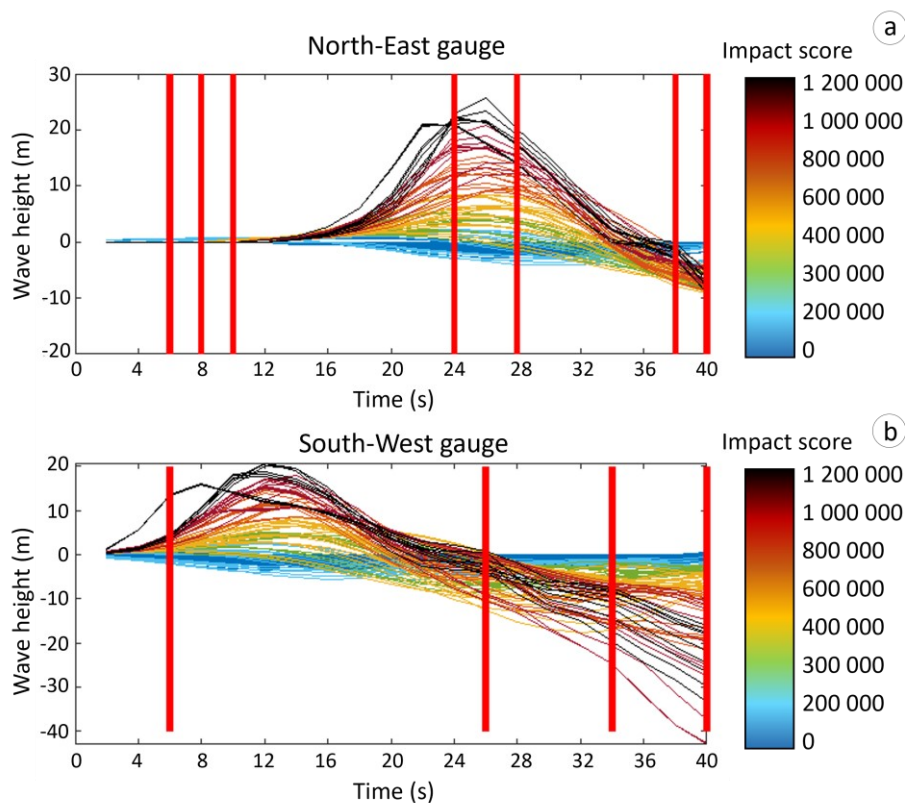
Figure 7: Gauge signals with a) North-East gauge and b) South-West gauge. The colour code corresponding to the impact score (in m² inundated). The bold red lines correspond to the 11 explanatory variables retained by the LASSO linear regression model.

To refine this relationship between wave amplitude and impact score, two approaches were adopted (see Methods and Appendix A). The first "rough" approach is a simple linear regression, i.e., we take the maximum amplitude value and relate it to the impact score (Figure 8a). With this approach some tsunamis with high impact scores are underestimated because the score predicted by the gauge is lower than the score determined by the inundation models (see orange ellipse in Figure 8a). In the second method, the LASSO penalised linear regression algorithm automatically chooses which gauge data values are most likely to explain the impact scores. The method finds 11 "explanatory variables" that best explain the relationship between gauge data and impact scores (Figure 7). The LASSO regression shows a closer relationship between the gauge data and impact scores than the simple regression and does not underestimate any tsunami with a high impact score (Figure 8b). The LASSO regression also results in small errors defining a linear relation with a low degree of scatter.
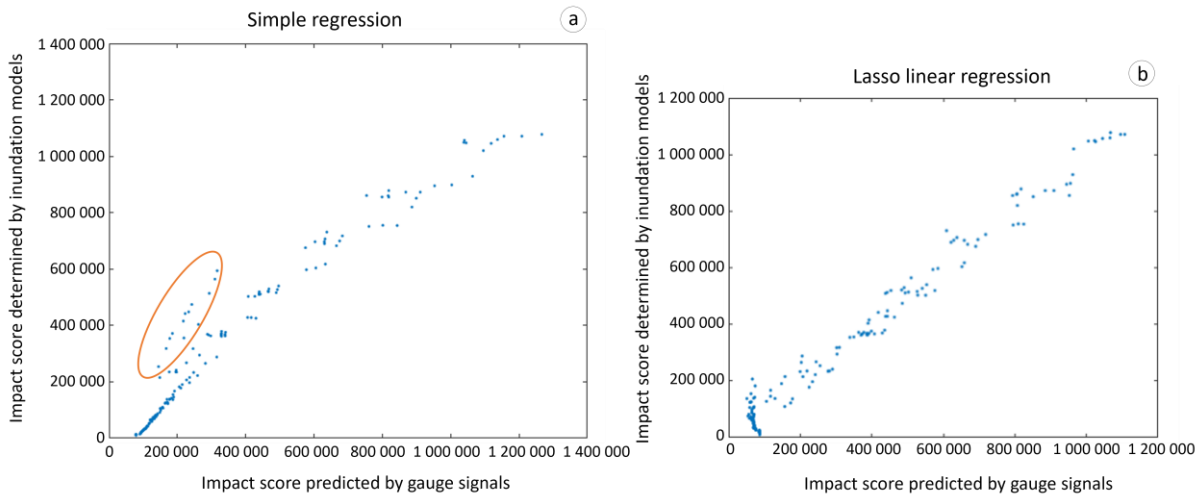
Figure 8: Inundation expected in m² by tsunami gauge signals according to a) a simple regression approach and b) a Lasso linear regression approach. Blues points represent each simulation of tsunamigenic landslide and orange ellipse represents tsunamis with a high impact score that are underestimated by the approach. The authors produced graphs by using MATLAB version 2019b.

3.4 Evacuation capacity

Evacuation modelling gives the fastest routes from each inundated pixel to a Refuge Area Entry Point (RAEP), i.e., an entry point into a safe zone. Results for Piscità, the most proximal community to the source, are given in Fig. 9 by way of example. Results for the Ficogrande, Punta Lena and Scari are given in Appendices B1, B2 and B3. As evacuation speeds consider slope and nature of the escape route (path width, surface type, presence of steps, etc.), some routes are not used because, although they appear short they are slow. This explains why RAEP4 and RAEP9 in Piscità (Figure 9), as well as RAEP12 in Ficogrande (Appendix B1), RAEP15 in Punta Lena (Appendix B2), and AEP22 in Scari (Appendix B3), are not chosen as viable Refuge Area Entry Points.

We considered the "evacuability" of each pixel in the inundated zones using the time for the wave to arrive (T_{arrive}) minus the time needed to travel between the pixel centroid and the closest, in terms of time, RAEP (evacuation time, T_{evac}). A positive difference for $T_{arrive} - T_{evac}$ thus means that the pixel can be evacuated for the given scenario, these being the green centroids in Figure 9, and Appendices B1, B2, and B3. Instead, a negative $T_{arrive} - T_{evac}$ means that the pixel cannot be evacuated in time, these being the red centroids in Figure 9, and Appendices B1, B2, and B3.
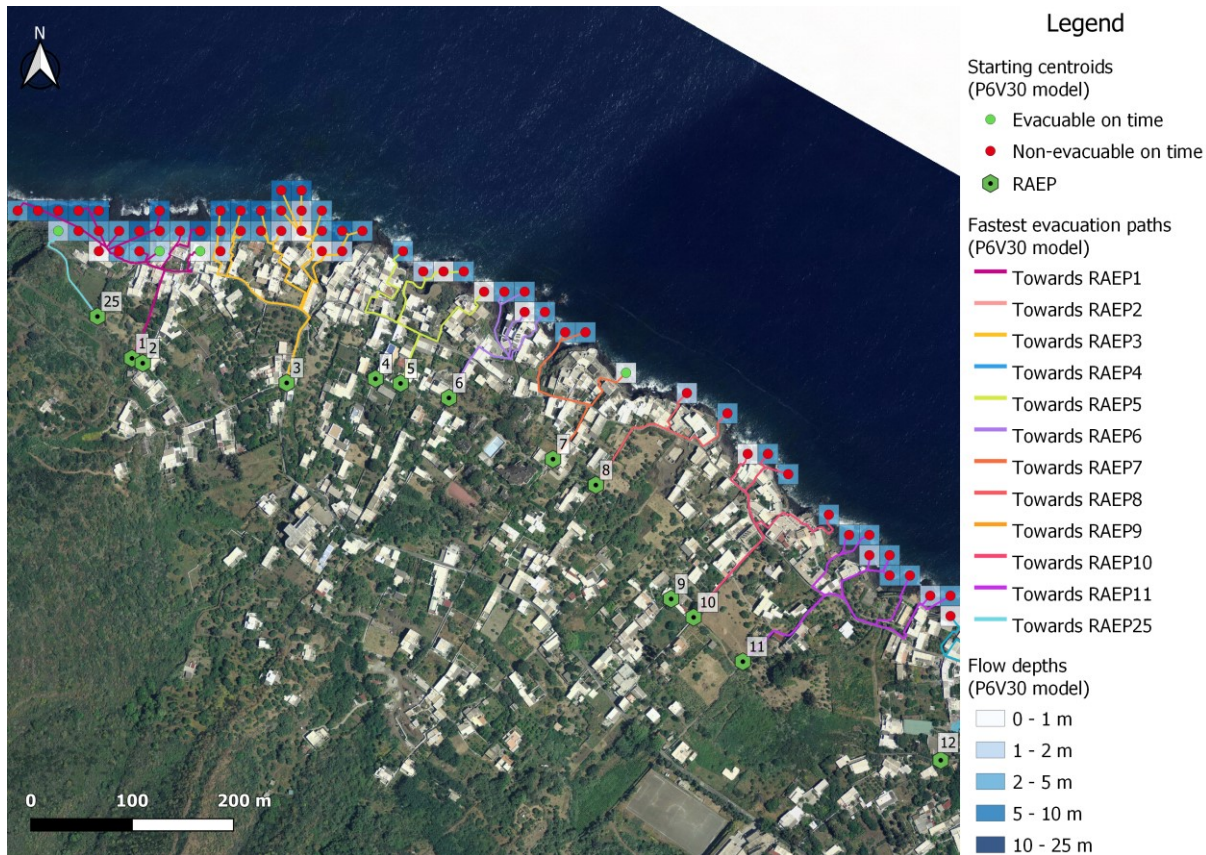
**Figure 9: Example of an evacuation model at Piscità created for a numerical simulation with a tsunamigenic landslide of 30 million m³ having broken away from position 6 (294 m below sea level) with a density of volcanic materials of 2.5 kg/m³. 64 pixels will be inundated (25 600 m²) with their associated flow depth, and the fastest evacuation routes. In green, points that can evacuate before the tsunami arrives and in red, points that cannot evacuate in time. The authors produced maps by using Quantum GIS version 3.16.7 software (2021).**

In our selected simulation example (scenario-P6V30CD0.4), out of 544 inundated pixels (217 600 m²), only 132 (24 %) pixels (52 800 m²) are theoretically capable of evacuation in time (i.e., the RAEP can be reached before the tsunami arrives). To understand if these pixels really can be evacuated before the arrival of the tsunami, we compared the warning times (minimum and maximum) available from the tsunami detection gauges and the warning times (minimum and maximum) needed to evacuate the inundated area (Figure 10). In terms of number of inundated pixels, we observe that for Piscità, Punta Lena and Scari there is time to evacuate some pixels but not the whole area (warning time needed > real warning time). To evacuate the whole area, a maximum of 102 seconds of extra warning time is needed for Piscità, 174 seconds for Punta Lena, and 368 seconds for Scari. For Ficogrande the two curves "warning time needed" and "real warning time" are very close (Figure 10), which means that most pixels can be evacuated before the wave arrives. At most an extra 41 seconds are needed to evacuate the whole area.

In terms of pixels
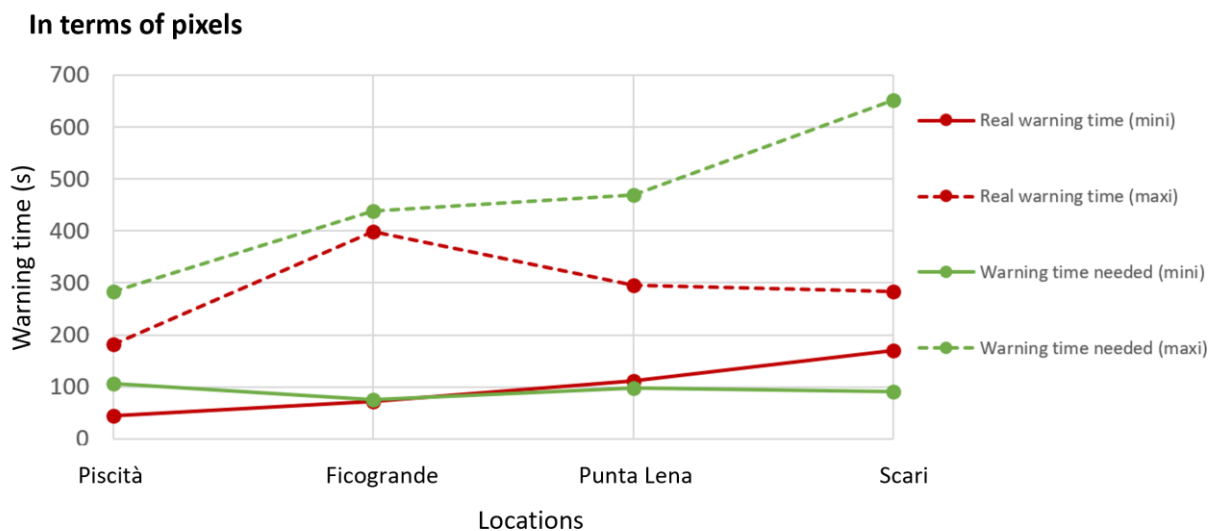
Figure 10: Minimum and maximum real warning time given by the tsunami gauges and warning time needed for each district to evacuate from the coastal inundated area.

295   In Figure 11 we assess the time needed to evacuate 25%, 50%, 75%, and 100% of the population from the inundated zone, and thus the warning time needed to complete partial or full evacuation. In doing this, we need to distinguish between an evacuation in winter and one in summer. In summer when the coastline if highly populated, differences in the time needed to evacuate 25%, 50%, 75%, and 100% of the population can be observed depending on time of day (Figure 11).

We see in Figure 11 the time of day during which evacuation is most effective varies from district to district. For example,

300   for Ficogrande the best time is day time when tourists gather in locations with easy access to RAEP13. Instead for Scari and Punta Lena all times of day are equally bad due to the long distances to the RAEPs. For Piscità, the situation is slightly better during the night when people leave the highly exposed beach and gather in the village closer to RAEPs. The situation is exacerbated in Piscità to due to its proximal location and thus the very short wave arrival time.

17
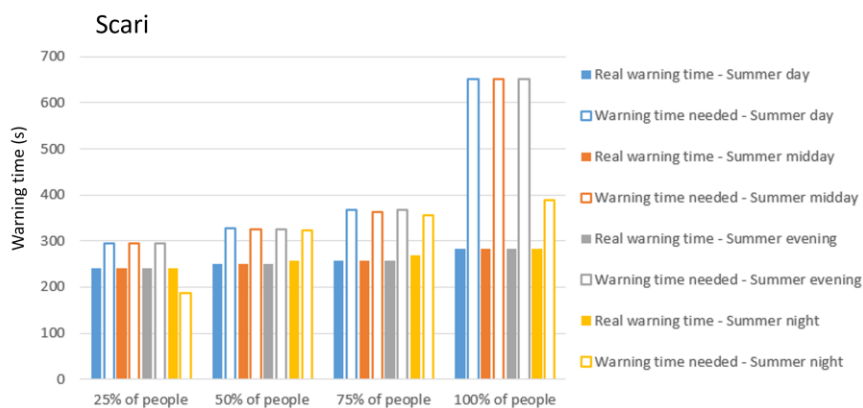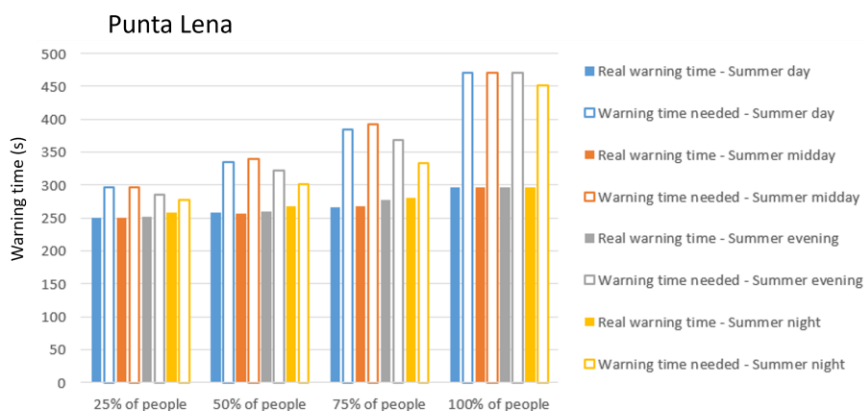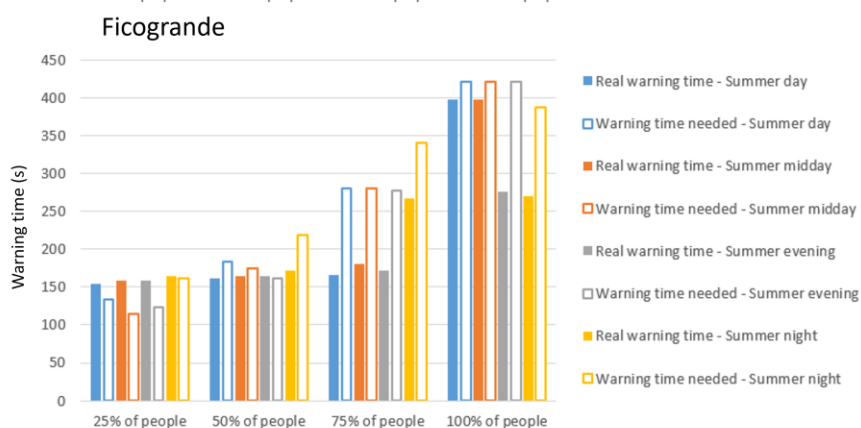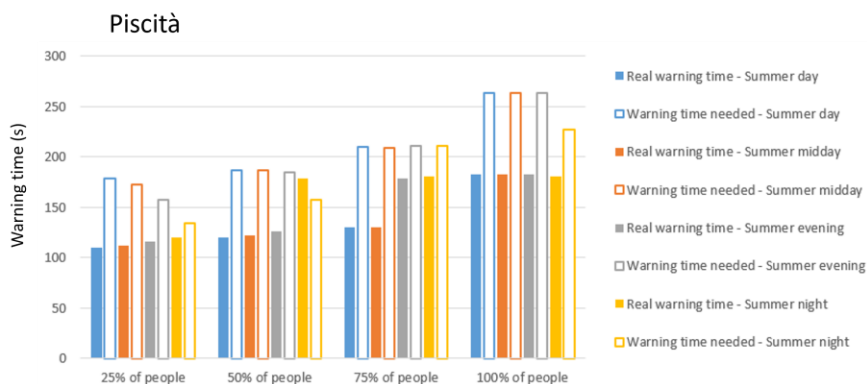
305 **Figure 11: Comparison between real warning time given by the tsunami gauges and warning time needed to evacuate 25%, 50%, 75% and 100% of Stromboli population from the four main inundated districts.**

To summarize the evacuation capacity of the zone inundated by scenario-P6V30CD0.4, we created histograms giving the distribution between the number of agents that can and cannot reach a RAEP depending on season and time of day (Figure 12). For this scenario, it is extremely difficult to evacuate on time. Out of 544 inundated pixels (217 600 m²), in the best case

310 (a tsunami occurring during a summer night), only 30% of population can evacuate (Figure 12). We also prepared individual histograms for each of the four main neighbourhoods of Stromboli village (see Appendices C1, C2, C3, and C4). Depending on the district, we can see that during certain periods of the year, and of the day, some are areas not occupied (i.e., their histograms have empty columns). This is particularly the case during the winter period, where a "winter desert" can be found in the districts of Piscità and Ficogrande, which are the locations of summer rentals, B&Bs and hotels. Unfortunately,

315 permanent residents are concentrated in the districts of Punta Lena and Scari, with Punta Lena being a zone with mainly non evacuable (red) points (Appendix B2). This explains why a winter night tsunami, when the Punta Lena population are at home and close to the shore, the evacuation capacity is 0 % (Appendix C3).

NUMBERS	EVACUATING ON TIME	NOT EVACUATING ON TIME		PERCENTAGES	EVACUATING ON TIME	NOT EVACUATING ON TIME
SUMMER DAY	135	663		SUMMER DAY	17	83
SUMMER MIDDAY	141	489		SUMMER MIDDAY	22	78
SUMMER EVENING	206	535		SUMMER EVENING	28	72
SUMMER NIGHT	199	460		SUMMER NIGHT	30	70
WINTER DAY	6	30		WINTER DAY	17	83
WINTER MIDDAY	5	21		WINTER MIDDAY	19	81
WINTER EVENING	2	17		WINTER EVENING	11	89
WINTER NIGHT	2	13		WINTER NIGHT	13	87
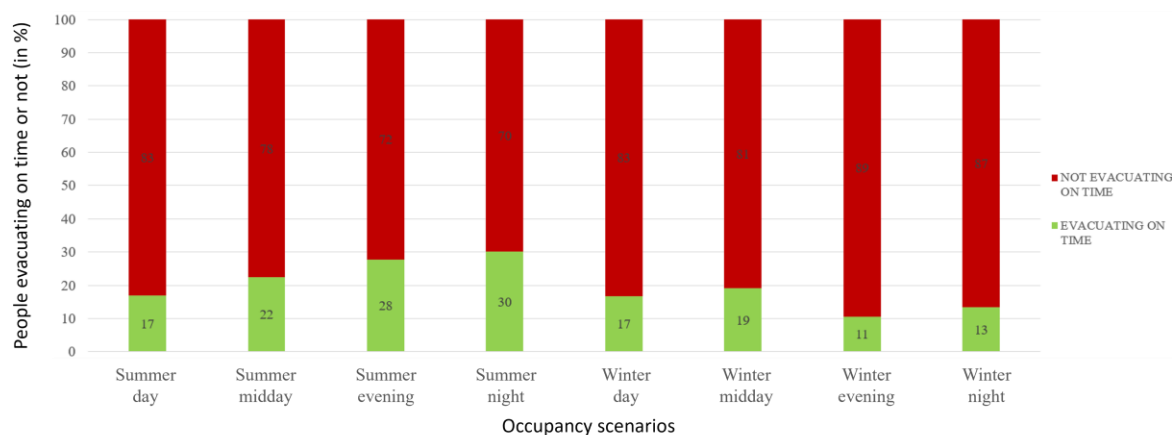
Figure 12: Table and histogram of the global number of people who can or cannot evacuate before the arrival of the tsunami in the
320 **case of a 30 million m³ tsunamigenic landslide at position 6 (294 m below sea level) with a density of volcanic materials of 2.5 kg/m³.**

19

4 Discussion

4.1 Landslide source parameters

The choice of the source input parameters was driven by the need of the Italian Civil Protection to analyse tsunami impacts in the range of the 2002 event (Tinti et al. 2006b). Larger events are possible (with the upper bound of the 1.81 km^3 mass
325   movement for the 5 ka event that formed the Sciara del Fuoco; Kokelaar & Romagnoli, 1995) and they are documented in the geological history of the island (Rosi et al., 2019; Pistolesi et al., 2020).

For what concerns the landslide initial positions, the highest impact is always associated with landslides triggered at the lowest subaerial positions (position 3, which is just above sea-level at 58 m a.s.l). This is due to the fact that granular flows starting at higher elevations deform and dilute during the downward motion, producing smaller waves. Finally, analysis of
330   the whole database allows us to state that the bulk density of the landslide has a second-order effect on its tsunamigenic capability. Our analysis, carried out on simulation-6 with a density contrast of 0.4, is substantially unchanged for lower densities.

Landslide position and volume are the key parameters in determining the hazard score. The dependency on other parameters such as landslide initial aspect ratio and horizontal position across the Sciara del Fuoco, are of second order. Numerical
335   simulations used in this work assume an initial position of the landslide along the central axis of the Sciara del Fuoco (consistently with the 2002 event). This assumption provides an average travel time for the tsunami to Stromboli village (Figure 1). Off-axis landslides will give longer or shorter travel times (by ±30 seconds) for the direction of Stromboli village depending on whether the landslide is in the western (furthest from the village) or eastern (closest to the village) sector of the Sciara del Fuoco, thus affecting the results of the evacuation model. However, this measure can be very sensitive to the wave
340   height, especially in areas characterized by small slopes or wall bounded regions (e.g., topographic pools). Future numerical investigations will sample initial landslide positions considering potential off-axis sources. Finally, it is worth remarking that different assumptions on the the granular flow rheology and water-landslide friction might significantly affect the results. Such effects will be analyzed in a dedicated, future work.

4.2 Human exposure

345   For the Aeolian Islands, demographic data are available from the official public census of 2021 (yearly survey by ISTAT, www.istat.it), and of 2011 (www.citypopulation.de). However, data are generally grouped by municipality for ISTAT, and by island and sometimes by district for Citypopulation.de. There are no data for the number of people living in each building, or their demographics. Thus, we had to rely on publicly available data, such as hotel booking forms on the internet, as well as ground-based census completed by us for permanently occupied houses in January 2020 (Bonilauri et al., 2021).
350   Some areas have therefore probably been over-estimated in terms of population capacity, under the assumption of full capacity for all holiday facilities during the summer season. Ideally, precise population distribution and demographic data

would allow us to adjust our evacuation model, but we consider the data used useful in providing a worst-case (full capacity) scenario.

For our evacuation time calculations, we considered a "standard" person with an associated forced walking speed (see Table
355   1; Péroche, 2016; Bonilauri et al., 2021). These were calibrated and checked as valid during escape simulations carried out by us in January 2020. Obtaining data on the age and physical abilities of the Stromboli inhabitants would allow construction of evacuation plans tailored to the individuals' capacities (cf. Bonilauri et al., 2021). Our escape times also involve no reaction time: the reaction is immediate, spontaneous, and correct, meaning that the agent escapes immediately using the fastest route.

360   Provitolo et al (2015) presented two main behaviours in psychological reactions to imminent danger. The first was "instinctive" behaviour where panic or disbelief prevail, and "learned" behaviours where reactions to danger are taken in a reflective manner, adapted to the context and no longer instinctive. These learned behaviours can be found in preventive or spontaneous evacuations when the context is already known by the population and has been anticipated, and is likely the case for the resident populations (Bonilauri et al., 2021). However, visitors are likely to fall into "instinctive" category. This
365   poses a problem for risk management and mitigation. That is why risk awareness campaigns are organised in volcanic contexts by Italian Civil Protection for several years to reduce reaction times in the face of real danger among the visitor population.

Reaction time is hard to consider because it is specific to each person depending, for example, on knowledge, experience and familiarity with the hazard. Establishing the reaction time of both informed and un-informed agents present in vulnerable
370   areas when the sirens sound is thus our next focus and will allow us to factor this uncertainty into our evacuation models. The same tests will allow us to assess, and refine, the escape times.

In winter, tourism on the island of Stromboli is greatly reduced with visitors numbering less than 5 per day, rising to 20 for two nights when a visiting football team was on the island (based on our January 2020 survey). Thus, generally, only permanent residents are present in the winter months, which numbered 98 during our January 2020 count. Because most of
375   the population live along the upper roads in the village, under winter conditions only around 20 residents are in vulnerable zones (mostly Punta Lena). However, these zones are at high risk with only an 11–13 % escape percentage on a winter evening or night (Figure 12), and thus require special attention in terms of evacuation needs.

The real warning time available to us (given by beacons) to evacuate as many people as possible before the tsunami reaches the coast is extremely short due to the short (<5 km) distance between source and point of impact. This means, that even for
380   the best case scenario, only 30% of the vulnerable population can be evacuated in time (Figure 12). As the warning time cannot be reduced, only accelerating the evacuation can guarantee the safety of the people living on or visiting the island.

Moreover, the greater the volume of the landslide is, the higher and faster the tsunami generated will be, reducing the warning time. Thus, this highlights the need to link tsunami waveforms to impact scores, and tailor evacuation times accordingly.

385 To speed up horizontal evacuation the number of, and ease of access to RAEPs, is necessary, as is distribution of evacuation plans and installation of signage. However, in cases where horizontal evacuation is clearly identified as impossible, vertical evacuation capable of taking the required capacity is the only solution (Bonilauri et al., 2021; Turchi et al., 2022). Since the response needs to be evacuation, either vertical or horizontal (Leone et al., 2013; Leone et al., 2018; Péroche, 2016; Solís and Gazmuri, 2017), the evacuation plans need to be developed well in advance. Our approach can be used to identify zones

390 suitable for horizontal and vertical evacuation, and be used to set capacity.

4.3 Anticipated inundation

The use of the LASSO penalised method (see Method; Figure 8; Appendix A) to link a beacon signal to a predicted inundation extent is a major advance in our tsunami risk assessment and management. Testing this method on real tsunami detection beacon signals instead of simulated signals would make it possible to determine if the method is valid and reliable

395 in real conditions, and eventually integrating it directly into the beacon algorithms would make it possible to estimate the impact zone before the tsunami reaches the inhabited coast. Having an estimation on how much coastline will be inundated, and therefore needs to be evacuated could also aid in disaster planning and management, as well as guiding search and rescue follow-up. The refuge area entry points could be automatically adapted to each tsunami case by lowering them in elevation for small tsunamis and raising them in elevation for larger tsunamis. In our current study, we considered two types

400 of RAEPs: 15 m a.s.l for smaller tsunamis and 35-40 m a.s.l for larger ones. This would modulate the population in need of evacuation, and regulate the load on escape routes, which could be blocked for agents at risk lower in the zone by agents in the upper zone undergoing an un-necessary evacuation. Such an approach allows output of the hazard maps and risk assessments in a real time, tailored to the case in hand.

5 Conclusion

405 At Stromboli, except the two tsunamis of December 2002, other landslide-related tsunamis have little or no data available. In such cases, hazard scenarios must be supported by modelling, validated by the well-constrained cases. The same can be argued for vulnerability and modelling of mitigation efforts, such as evacuation, where gaps need to be identified and filled through extrapolation. Our integrated modelling approach, which involves a statistical combination of model-output hazard metrics (wave run up, arrival time and sea floor pressure sensor waveform), with a seasonally and diurnally distributed

410 populations plus a model for evacuation times, allows risk mapping to assess whether a point is capable of horizontal evacuation or not.

The simulated scenarios allow us to consider a wide range of source conditions, enabling for a statistical approach to hazard assessment and providing scenario-tailored evacuation maps. Our approach involves 156 hazard (tsunami) scenarios and five diurnal (morning, midday, afternoon, evening, and night) population distributions divided by season (winter and summer).

415 This results in $156 \times 5 \times 2$ combinations of risk assessment scenarios. Each risk assessment scenario can be linked to the tsunamic type through the waveform recorded by a sea floor pressure gauge, and automatically selected accordingly. Given a warning time of less than a 3–6 minutes on a small volcanic island where the tsunami source is just few kilometres from the vulnerable, shoreline population, such a pre-prepared and automatic event outcome procedure is indispensable.

This method is tested and applied here to the Stromboli, but it can serve as a blueprint for any other volcanic island where

420 volcanic activity and landslides cause local tsunamis with little warning time. Key elements in this are to collect the two most important source terms for hazard modelling (landslide location and volume) as well as spatial and temporal assessments of population distributions. Given uncertainty in the source terms and population distributions our scenario-based approach considers that all simulations have the same probability of future occurrence, as well as a worst case scenario for population distribution. This approach is thus consistent with the precautionary principle of disaster management, while

425 being open to refinement subject to further data collection from, for example, geological studies, expert elicitation, evacuation tests and/or population surveys, which is our next step.

Appendices

Appendix A. Statistical analysis of tsunamigenic landslides and penalised linear regression LASSO.

Our aim is to define a tsunami impact score based on the coastal inundation, and to understand the link between this score,

430 the associated landslide characteristics, and the gauge signals.

For each tsunamigenic landslide i (i.e., individual i) we have:

- The landslide characteristics given by (V_i, P_i, D_i), where V_i is the volume of volcanic material, P_i is the onset position of the landslide along the Sciara del Fuoco, and D_i is the density of the landslide material.

- The area of coastal inundation described by a vector $X_i = (x_{(i,1)}, \ldots, x_{(i,j)}, \ldots, x_{(i,31635)})$ of 31635 values (i.e., the number of

435 pixels of the DEM) of 0 or 1, $x_{i,j} = 1$ if the jth pixel is inundated by the tsunami generated by the landslide i.

- The associated gauge signals BNE_i and BSW_i, which are two vectors describing the wave heights recorded every 2 seconds since the beginning of the landslide.

For each scenario, the inundation is given by a map of high dimensional data (dimension is 31635 values). To reduce the data dimension, we tested three classical statistical methods (PCA, Multidimensional Scaling, and Isomap), and we found 440   that the inundation data is very close to a one-dimensional space characterized by the total number of inundated pixels.

Since we have data for 156 simulations, we used a regression model to reduce the number of scenarios by searching for a relationship between the explanatory variables and the variables to be explained of the type $Y = f(X_1, ..., X_k) + \varepsilon$, we usually look for the "best" function f within a family of function parameters (e.g., for polynomials of degree less than d, then d is the parameter). Due to the high dimensionality (relatively to the number of experiment) we have evaluated two 445   approaches: (1) a rough approach, i.e., retaining only the maximum amplitude on the first major wave detected by each gauge, and (2) a more classical approach which consists in applying a Lasso penalised linear regression to select a smaller number of explanatory variables (Giraud, 2021).

The purpose of a multiple regression is to explain a variable y belonging to $\mathbb{R}$ using p explanatory variables $x_1, ..., x_p$ also in $\mathbb{R}$. In our case, y is the hazard score and $x_1, ..., x_p$ are the signals emitted by the two tsunami detection beacons.

450   1. The linear regression

It is assumed that y can be determined as a function of $x_1, ..., x_p$ in a linear way, i.e., that there is an affine function f such as:

$$y = f(x_1, ..., x_p) = a_1 x_1 + ... + a_p x_p + b + \varepsilon$$

$a_1, ..., a_p$ and b are the unknown coefficients that we will try to estimate from measurements made on individuals. In our case, an individual is a tsunamigenic landslide scenario.   The random part ε synthesises the measurement noise and the 455   experimental uncertainties.

For each individual i we measure Y_i the value of the variable y and $X_{1,i}, ..., X_{p,i}$ the values of the variables x_1 to x_p.

To carry out a linear regression is to look for coefficients $\hat{a}_1, ..., \hat{a}_p$, and $\hat{b}$ which best allow us to estimate $\hat{a}_1, ..., \hat{a}_p$, and $\hat{b}$ from the results of our N individuals.

For this purpose, we define for each individual i:

460    $\hat{Y}_i (\alpha_1, ..., \alpha_p, \beta) = \alpha_1 X_{1,i} + .. + \alpha_p X_{p,i} + \beta$

If $\alpha_1 = a_1$, $\alpha_p = a_p$, $\beta = b$ and $\varepsilon = 0$ then $Y_i = \hat{Y}_i (\alpha_1, ..., \alpha_p, \beta)$ and $|\hat{Y}_i - Y_i| = 0$.

We can show that there is equivalence between: "the α_i are all close to a_i and β is close to b" and that "all $\hat{Y}_i$ are close to Y_i".

24

This is why the coefficients $\hat{a}_1$, ..., $\hat{a}_p$, and $\hat{b}$ calculated in a linear regression are those that make the error criterion: $\sum (\hat{Y}_i (\alpha_1, \ldots, \alpha_p, \beta) - Y_i)^2$ minimum.

465   Linear regression does not fit the two situations:

- If N (total number of experiments done) ≤ p (total number of explanatory variables), i.e., when there are fewer experiments than the number of explanatory variables.

- Explanatory variables are too correlated.

Our problem lies in both cases so we cannot use classical linear regression.

470   2.   Lasso penalised linear regression

There are ways to get around the limitations of linear regression. One of them is the LASSO penalty. LASSO is described and studied in the book "Introduction to High-Dimensional Statistics" by Christophe Giraud (2021) in which it has been proven that this penalty works and is adequate to solve problems similar to ours.

The LASSO penalty consists in adding to the error criterion of the linear regression, a penalty proportional to the sum of the
475   absolute values of the coefficients. This has the effect of cancelling many coefficients (which means working on fewer variables and therefore limits the negative effects of the above-mentioned situations).

The criterion to be minimised becomes $\sum (\hat{Y}_i (\alpha_1, \ldots, \alpha_p, \beta) - Y_i)^2 + \lambda (|\hat{b}| + \sum |\hat{a}i|)$.

For each λ value we have an associated lasso regression. To choose a λ value one can use classical "model choice" methods. For our part, we used the "Leave one out" method thanks to the parameter selection program present in the MATLAB
480   software.

The "Leave one out" method applied to our case gives:

For a λ:

- For each i (one of our tsunamigenic landslide scenarios),

- virtually remove individual i from our experiments (we pretend we have no information for individual i);

485   - apply the LASSO method to calculate the coefficients ($\hat{a}_1$, ..., $\hat{a}_p$, and $\hat{b}$) on all other individuals;

- calculate $\hat{Y}_i*$ the estimated value of Y_i from the previously estimated coefficients then $E_i(\lambda) = (\hat{Y}_i* - Y_i)^2$.

The error associated with lambda is defined by $E(\lambda) = \sum E_i(\lambda)$

Start again with several values of λ and choose the λ making $E(\lambda)$ minimum.

490 **Appendix B.** Examples of evacuation model at Ficogrande (B1), Punta Lena (B2), and Scari (B3) created for a numerical simulation with a tsunamigenic landslide of 30 million m³ having broken away from position 6 (294 m below sea level) with a density of volcanic materials of 2.5 kg/m³. Here the pixels that will be inundated and their associated flow depth, and the fastest evacuation routes. In green, points that can evacuate before the tsunami arrives and in red, points that cannot evacuate in time. The authors produced maps by using Quantum GIS version 3.16.7 software (2021).
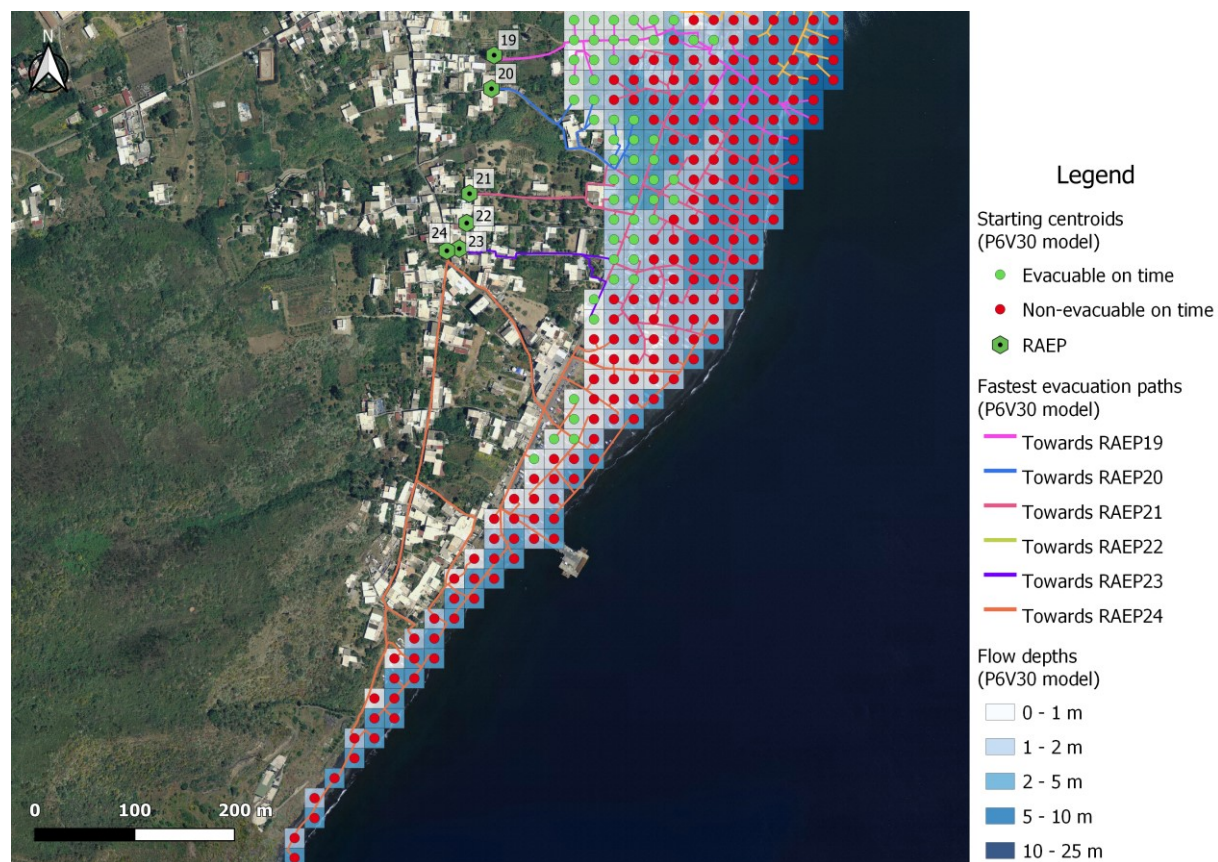
495 **(B1) Ficogrande – 79 inundated pixels (31 600 m²)**
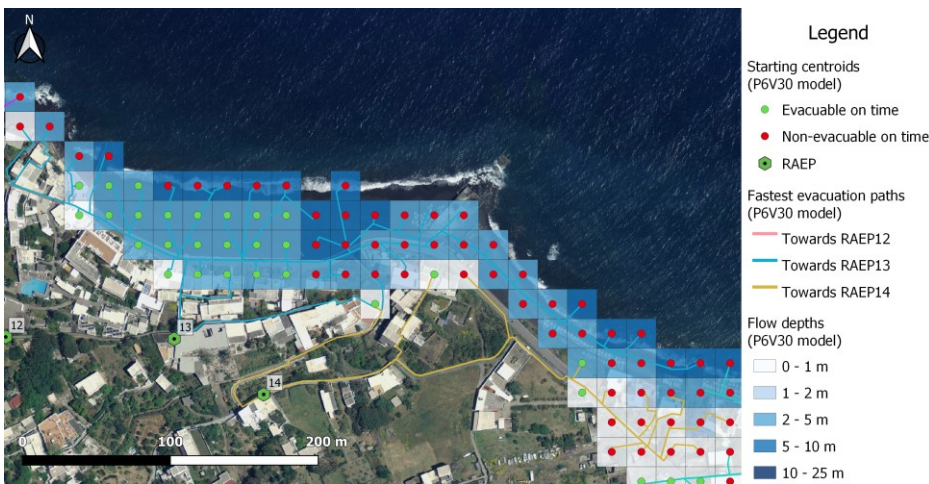
(B2) Punta Lena – 178 inundated pixels (71 200 m²)
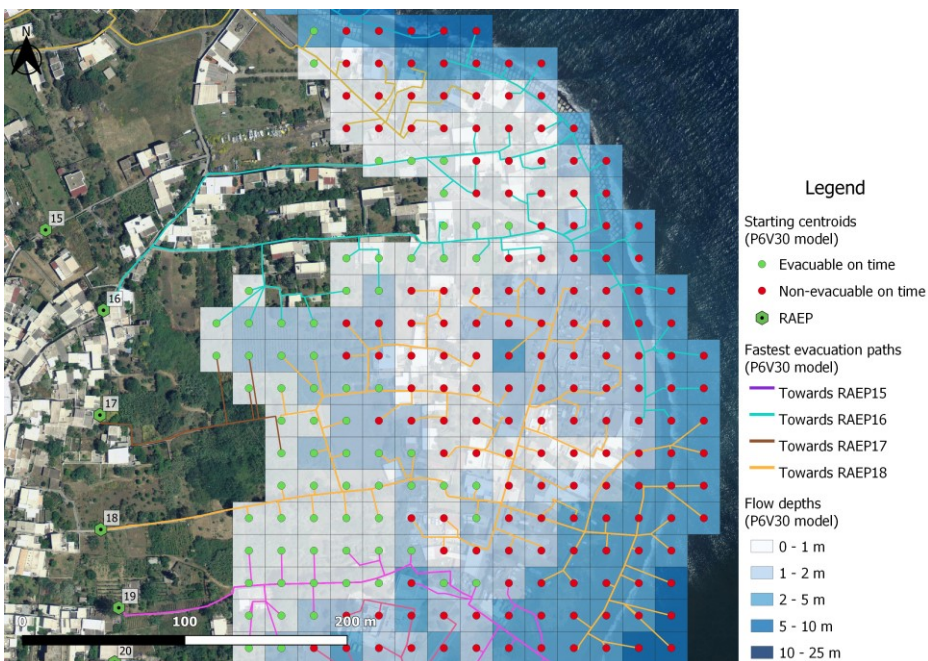
**(B3) Scari – 223 inundated pixels (89 200 m²)**

500

Appendix C. Table and histogram, for Piscità (C1), Ficogrande (C2), Punta Lena (C3), and Scari (C4), of the global number of people who can or cannot evacuate before the arrival of the tsunami in the case of a 30 million m³ tsunamigenic landslide at position 6 (294 m below sea level) and with a density of volcanic materials of 2.5 kg/m³.
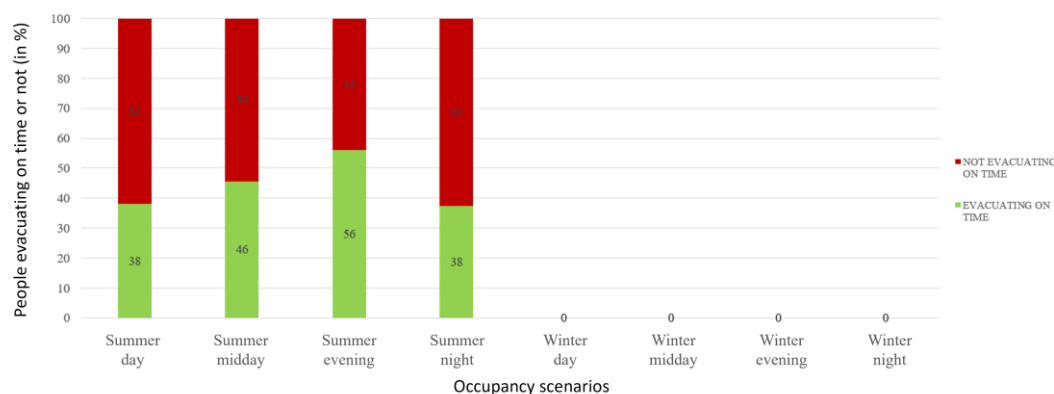
505 **(C1) Piscità – 64 inundated pixels (25 600 m²)**

NUMBERS	EVACUATING ON TIME	NOT EVACUATING ON TIME	PERCENTAGES	EVACUATING ON TIME	NOT EVACUATING ON TIME
SUMMER DAY	2	115	SUMMER DAY	2	98
SUMMER MIDDAY	2	43	SUMMER MIDDAY	4	96
SUMMER EVENING	13	58	SUMMER EVENING	18	82
SUMMER NIGHT	27	41	SUMMER NIGHT	40	60
WINTER DAY	0	1	WINTER DAY	0	100
WINTER MIDDAY	0	0	WINTER MIDDAY	0	0
WINTER EVENING	0	0	WINTER EVENING	0	0
WINTER NIGHT	0	0	WINTER NIGHT	0	0
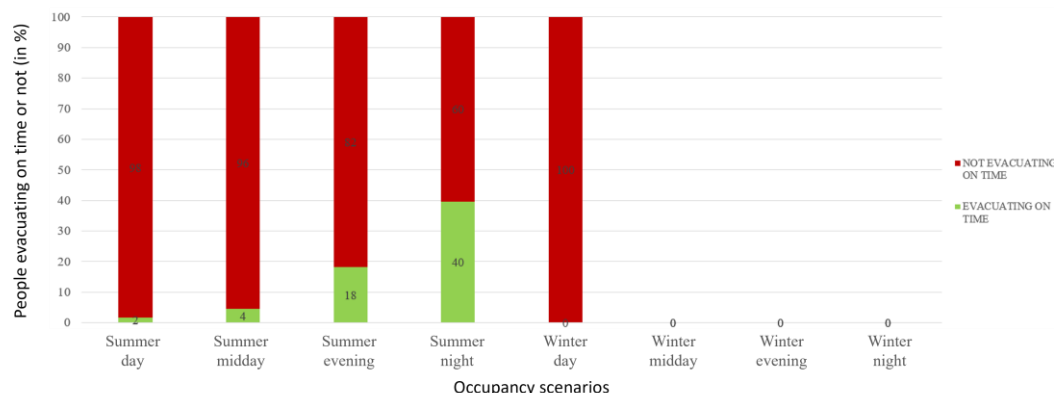
(C2) Ficogrande – 79 inundated pixels (31 600 m²)

NUMBERS	EVACUATING ON TIME	NOT EVACUATING ON TIME	PERCENTAGES	EVACUATING ON TIME	NOT EVACUATING ON TIME
SUMMER DAY	48	78	SUMMER DAY	38	62
SUMMER MIDDAY	74	88	SUMMER MIDDAY	46	54
SUMMER EVENING	119	93	SUMMER EVENING	56	44
SUMMER NIGHT	78	130	SUMMER NIGHT	38	63
WINTER DAY	0	0	WINTER DAY	0	0
WINTER MIDDAY	0	0	WINTER MIDDAY	0	0
WINTER EVENING	0	0	WINTER EVENING	0	0
WINTER NIGHT	0	0	WINTER NIGHT	0	0

29

(C3) Punta Lena – 178 inundated pixels (71 200 m²)

NUMBERS	EVACUATING ON TIME	NOT EVACUATING ON TIME	PERCENTAGES	EVACUATING ON TIME	NOT EVACUATING ON TIME
SUMMER DAY	28	134	SUMMER DAY	17	83
SUMMER MIDDAY	25	122	SUMMER MIDDAY	17	83
SUMMER EVENING	34	152	SUMMER EVENING	18	82
SUMMER NIGHT	57	203	SUMMER NIGHT	22	78
WINTER DAY	2	10	WINTER DAY	17	83
WINTER MIDDAY	1	10	WINTER MIDDAY	9	91
WINTER EVENING	0	6	WINTER EVENING	0	100
WINTER NIGHT	0	6	WINTER NIGHT	0	100
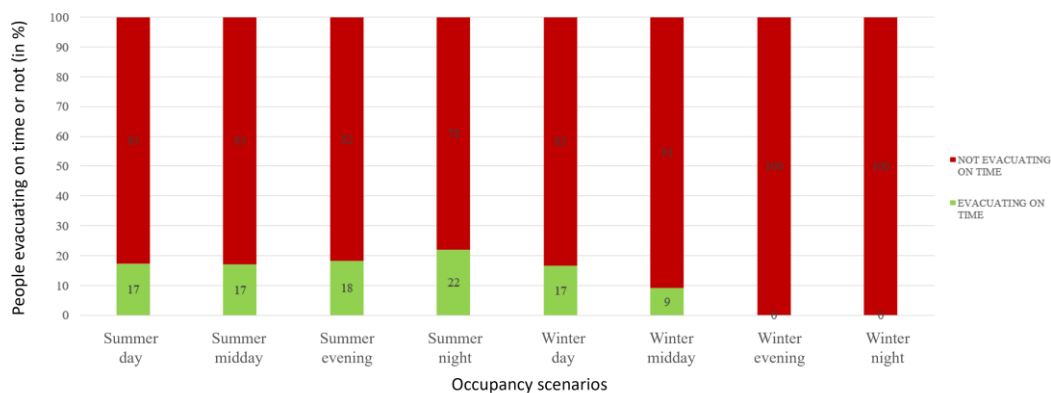
510

(C4) Scari – 223 inundated pixels (89 200 m²)

NUMBERS	EVACUATING ON TIME	NOT EVACUATING ON TIME	PERCENTAGES	EVACUATING ON TIME	NOT EVACUATING ON TIME
SUMMER DAY	57	337	SUMMER DAY	14	86
SUMMER MIDDAY	40	239	SUMMER MIDDAY	14	86
SUMMER EVENING	40	233	SUMMER EVENING	15	85
SUMMER NIGHT	37	87	SUMMER NIGHT	30	70
WINTER DAY	4	19	WINTER DAY	17	83
WINTER MIDDAY	4	11	WINTER MIDDAY	27	73
WINTER EVENING	2	11	WINTER EVENING	15	85
WINTER NIGHT	2	7	WINTER NIGHT	22	78

515

30
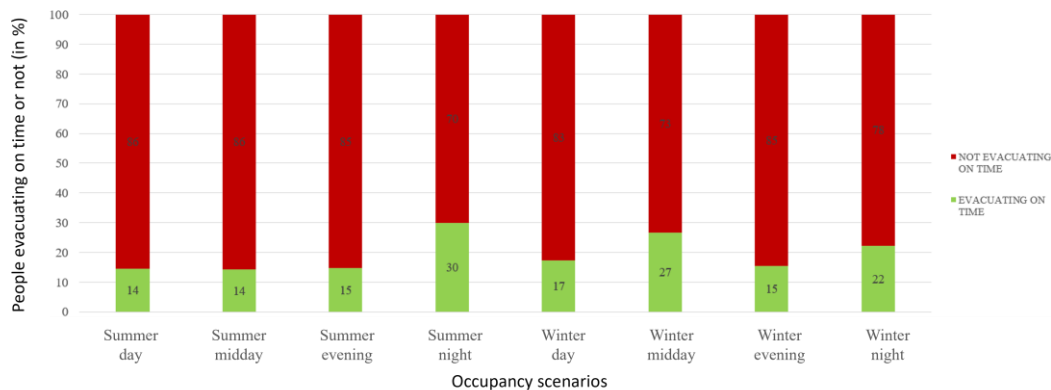
Availability of data and materials

All maps produced as part of work of Emmie M. Bonilauri are available on request, but the GIS is property of DPC and is thus only available for situations involving officially sanctioned access and collaboration. The database of numerical simulations is available at XXXX.

520

Funding

This work was completed as part of E.B PhD funded by the French government IDEX-ISITE initiative16- IDEX-0001 (CAP 20–25).

525 **Statements and Declarations**

This work was supported under the 2012-2021 agreement between Istituto Nazionale di Geofisica e Vulcanologia (INGV) and the Italian Presidenza del Consiglio dei Ministri, Dipartimento della Protezione Civile (DPC), Convenzione B2, WP2 Task 12 (2019-2021).

530 **Authors' contributions**

EB was responsible for all data processing and analysis through set up of the GIS and its data layers. MC, BC, TEO completed all tsunami modelling and provided the hazard data layers. CA guided development and application of the statistical methodologies. RP and AH conceptualised designed and guided the work. DM ensured the results were applicable to the field needs of Civil Protection. EB led manuscript figure and table preparation with input from all co-authors.

535

Competing interests

The authors declare that they have no competing interests.

Acknowledgements

540 E.B acknowledges the support of the French government IDEX-ISITE initiative16- IDEX-0001 (CAP 20–25) and the whole group acknowledge the support from Italian Civil Protection through contract XXXXX. This is CLERVOLC publication n°XXXXX.

References

Acocella, V., Neri, M., and Scarlato, P.: Understanding shallow magma emplacement at volcanoes: Orthogonal feeder dikes
545 during the 2002–2003 Stromboli (Italy) eruption, Geophysical Research Letters, 33, https://doi.org/10.1029/2006GL026862, 2006.

Boldini, D., Wang, F., Sassa, K., and Tommasi, P.: Mechanism of Landslide Causing the December 2002 Tsunami at Stromboli Volcano (Italy), in: Landslides: Risk Analysis and Sustainable Disaster Management, edited by: Sassa, K., Fukuoka, H., Wang, F., and Wang, G., Springer, Berlin, Heidelberg, 173–180, https://doi.org/10.1007/3-540-28680-2_21, 550   2005.

Bonaccorso, A., Calvari, S., Garfì, G., Lodato, L., and Patanè, D.: Dynamics of the December 2002 flank failure and tsunami at Stromboli volcano inferred by volcanological and geophysical observations, Geophysical Research Letters, 30, https://doi.org/10.1029/2003GL017702, 2003.

Bonilauri, E. M., Harris, A. J. L., Morin, J., Ripepe, M., Mangione, D., Lacanna, G., Ciolli, S., Cusolito, M., and Deguy, P.: 555   Tsunami evacuation times and routes to safe zones: a GIS-based approach to tsunami evacuation planning on the island of Stromboli, Italy, Journal of Applied Volcanology, 10, 4, https://doi.org/10.1186/s13617-021-00104-9, 2021.

Calvari, S., Spampinato, L., Lodato, L., Harris, A. J. L., Patrick, M. R., Dehn, J., Burton, M. R., and Andronico, D.: Chronology and complex volcanic processes during the 2002–2003 flank eruption at Stromboli volcano (Italy) reconstructed from direct observations and surveys with a handheld thermal camera, Journal of Geophysical Research: Solid Earth, 110, 560   https://doi.org/10.1029/2004JB003129, 2005.

Calvari, S., Branca, S., Corsaro, R. A., De Beni, E., Miraglia, L., Norini, G., Wijbrans, J., and Boschi, E.: Reconstruction of the eruptive activity on the NE sector of Stromboli volcano: timing of flank eruptions since 15 ka, Bull Volcanol, 73, 101–112, https://doi.org/10.1007/s00445-010-0412-5, 2011.

NCEI | Center NGD Tsunami Data and Information: https://www.ngdc.noaa.gov/hazard/tsu.shtml, last access 9 January 565   2023.

Chiocci, F. L., Bosman, A., Romagnoli, C., Tommasi, P., and de Alteris, G.: The December 2002 Sciara del Fuoco (Stromboli Island) submarine landslide: a first characterization, 12069, 2003.

Chiocci, F. L., Romagnoli, C., and Bosman, A.: Morphologic resilience and depositional processes due to the rapid evolution of the submerged Sciara del Fuoco (Stromboli Island) after the December 2002 submarine slide and tsunami, 570   Geomorphology, 100, 356–365, https://doi.org/10.1016/j.geomorph.2008.01.008, 2008a.

Chiocci, F., Romagnoli, C., and Tommasi, P.: The Stromboli 2002 tsunamigenic submarine slide: Characteristics and possible failure mechanisms, Journal of Geophysical Research, 113, https://doi.org/10.1029/2007JB005172, 2008b.

Chiocci, F. L. and Ridente, D.: Regional-scale seafloor mapping and geohazard assessment. The experience from the Italian project MaGIC (Marine Geohazards along the Italian Coasts), Mar Geophys Res, 32, 13–23, https://doi.org/10.1007/s11001-575   011-9120-6, 2011.

Citypopulation.de Stromboli (Messina, Sicily, Italy) - Population Statistics, Charts, Map, Location, Weather and Web Information: https://www.citypopulation.de/en/italy/localities/sicilia/messina/08304110011__stromboli/, last access 10 October 2023.

Esposti Ongaro, T., de' Michieli Vitturi, M., Cerminara, M., Fornaciai, A., Nannipieri, L., Favalli, M., Calusi, B., Macías, J., 580   Castro, M. J., Ortega, S., González-Vida, J. M., and Escalante, C.: Modeling Tsunamis Generated by Submarine Landslides

at Stromboli Volcano (Aeolian Islands, Italy): A Numerical Benchmark Study, Frontiers in Earth Science, 9, 274, https://doi.org/10.3389/feart.2021.628652, 2021.

Favalli, M., Fornaciai, A., and Pareschi, M. T.: LIDAR strip adjustment: Application to volcanic areas, Geomorphology, 111, 123–135, https://doi.org/10.1016/j.geomorph.2009.04.010, 2009.

585   Fernández-Nieto, E., Parisot, M., Penel, Y., and Sainte-Marie, J.: A hierarchy of dispersive layer-averaged approximations of Euler equations for free surface flows, Communications in Mathematical Sciences, 16, 1169–1202, https://doi.org/10.4310/CMS.2018.v16.n5.a01, 2018.

Fornaciai, A., Favalli, M., and Nannipieri, L.: Numerical simulation of the tsunamis generated by the Sciara del Fuoco landslides (Stromboli Island, Italy), Sci Rep, 9, 18542, https://doi.org/10.1038/s41598-019-54949-7, 2019.

590   Fornaciai, A., Favalli, M., and Nannipieri, L.: Reconstruction of the 2002 tsunami at Stromboli using the non-hydrostatic WAVE model (NHWAVE), Geological Society, London, Special Publications, 519, SP519-2020–162, https://doi.org/10.1144/SP519-2020-162, 2022.

Giordano, G. and De Astis, G.: The summer 2019 basaltic Vulcanian eruptions (paroxysms) of Stromboli, Bull Volcanol, 83, 1, https://doi.org/10.1007/s00445-020-01423-2, 2020.

595   Giraud, C.: Introduction to high-dimensional statistics and probability, 364 pp., https://doi.org/10.1111/rssa.12861, 2021.

Grezio, A., Babeyko, A., Baptista, M. A., Behrens, J., Costa, A., Davies, G. R., Geist, E. L., Glimsdal, S., González, F. I., Griffin, J., Harbitz, C. B., Leveque, R. J., Lorito, S., Løvholt, F., Omira, R., Mueller, C., Paris, R., Parsons, T., Polet, J., Power, W., Selva, J., Sørensen, M. B., and Thio, H. K.: Probabilistic Tsunami Hazard Analysis: Multiple Sources and Global Applications, Reviews of Geophysics, https://doi.org/10.1002/2017RG000579, 2017.

600   Harbitz, C., Løvholt, F., and Bungum, H.: Submarine landslide tsunamis: how extreme and how likely?, Natural Hazards: Journal of the International Society for the Prevention and Mitigation of Natural Hazards, 72, 1341–1374, https://doi.org/10.1007/s11069-013-0681-3, 2014.

Istat.it Dashboard Permanent census of population and housing: https://esploradati.censimentopopolazione.istat.it/databrowser/#/en/censtest/dashboards, last access 17 October 2023.

605   Kokelaar, P. and Romagnoli, C.: Sector collapse, sedimentation and clast population evolution at an active island-arc volcano: Stromboli, Italy, Bull Volcanol, 57, 240–262, https://doi.org/10.1007/BF00265424, 1995.

Lacanna G. and Ripepe M.: Genesis of tsunami waves generated by Pyroclastic flows and the Early-Warning system, The Rittmann Conference, Catania, Italy, ISSN 1590-2595, https://www.conferenzarittmann.it/images/2020/Miscellanea_52.pdf, 2020.

610   Leone, F., Péroche, M., Lagahé, E., Gherardi, M., Sahal, A., Vinet, F., Hachim, S., and Lavigne, F.: Modélisation de l'accessibilité territoriale pour l'aide à la gestion de crise tsunami (Mayotte, France), Annales de géographie, 693, 502–524, https://doi.org/10.3917/ag.693.0502, 2013.

Leone, F., Péroche, M., Robustelli, M., Cargnelutti, L., Perdrieau, J.-C., Coupin, T., and Gherardi, M.: Planifier les évacuations en cas de tsunami : la méthode EXPLOIT, Guide méthodologique, Service des publications de Montpellier 3, 615 2018.

Macías, J., Escalante, C., and Castro, M. J.: Multilayer-HySEA model validation for landslide-generated tsunamis – Part 1: Rigid slides, Natural Hazards and Earth System Sciences, 21, 775–789, https://doi.org/10.5194/nhess-21-775-2021, 2021a.

Macías, J., Escalante, C., and Castro, M. J.: Multilayer-HySEA model validation for landslide-generated tsunamis – Part 2: Granular slides, Natural Hazards and Earth System Sciences, 21, 791–805, https://doi.org/10.5194/nhess-21-791-2021, 620 2021b.

Maramai, A., Graziani, L., Alessio, G., Burrato, P., Colini, L., Cucci, L., Nappi, R., Nardi, A., and Vilardo, G.: Near- and far-field survey report of the 30 December 2002 Stromboli (Southern Italy) tsunami, Marine Geology, 215, 93–106, https://doi.org/10.1016/j.margeo.2004.11.009, 2005a.

Maramai, A., Graziani, L., and Tinti, S.: Tsunamis in the Aeolian Islands (southern Italy): a review, Marine Geology, 215, 625 11–21, https://doi.org/10.1016/j.margeo.2004.03.018, 2005b.

Maramai, A., Graziani, L., and Brizuela, B.: Euro-Mediterranean Tsunami Catalogue (EMTC), version 1.0 (1.0), https://doi.org/10.13127/TSUNAMI/EMTC.1.0, 2014.

Muhari, A., Heidarzadeh, M., Susmoro, H., Nugroho, H. D., Kriswati, E., Supartoyo, Wijanarto, A. B., Imamura, F., and Arikawa, T.: The December 2018 Anak Krakatau Volcano Tsunami as Inferred from Post-Tsunami Field Surveys and 630 Spectral Analysis, Pure Appl. Geophys., 176, 5219–5233, https://doi.org/10.1007/s00024-019-02358-2, 2019.

Paris, R., Ramalho, R. S., Madeira, J., Avila, S. L., May, S. M., Rixhon, G., Engel, M., Brückner, H., Herzog, M., Schukraft, G., Perez-Torrado, F. J., Rodriguez-Gonzalez, A., Carracedo, J. C., and Giachetti, T.: Mega-tsunami conglomerates and flank collapses of ocean island volcanoes, Marine Geology, 395, 168–187, https://doi.org/10.1016/j.margeo.2017.10.004, 2018.

635 Péroche, M.: La gestion de crise tsunami dans la Caraïbe : contribution géographique aux dispositifs d'alerte et d'évacuation des populations, phdthesis, UNIVERSITÉ PAUL VALERY MONTPELLIER 3 PAUL-VALÉRY, 2016.

Pino, N. A., Ripepe, M., and Cimini, G. B.: The Stromboli Volcano landslides of December 2002: A seismological description, Geophysical Research Letters, 31, https://doi.org/10.1029/2003GL018385, 2004.

Pistolesi, M., Bertagnini, A., Di Roberto, A., Ripepe, M., and Rosi, M.: Tsunami and tephra deposits record interactions 640 between past eruptive activity and landslides at Stromboli volcano, Italy, Geology, 48, 436–440, https://doi.org/10.1130/G47331.1, 2020.

Provitolo, D., Dubos-Paillard, E., Verdière, N., Lanza, V., Charrier, R., Bertelle, C., and Aziz-Alaoui, M. A.: Les comportements humains en situation de catastrophe : de l'observation à la modélisation conceptuelle et mathématique, Cybergeo : Revue européenne de géographie / European journal of geography, https://doi.org/10.4000/cybergeo.27150, 645 2015.

Riskianingrum, D. and Yogaswara, H.: The fading of disaster memory in Pulau Sebesi: A historical construction, E3S Web Conf., 340, 05008, https://doi.org/10.1051/e3sconf/202234005008, 2022.

Rosi, M., Bertagnini, A., and Landi, P.: Onset of the persistent activity at Stromboli Volcano (Italy), Bull Volcanol, 62, 294–300, https://doi.org/10.1007/s004450000098, 2000.

650 Rosi, M., Pistolesi, M., Bertagnini, A., Landi, P., Pompilio, M., and Di Roberto, A.: Stromboli volcano, Aeolian Islands (Italy): present eruptive activity and hazards, in: The Aeolian Islands Volcanoes, vol. 37, edited by: Lucchi, F., Peccerillo, A., Keller, J., Tranne, C. A., and Rossi, P. L., Geological Society of London, 0, https://doi.org/10.1144/M37.14, 2013.

Selva, J., Amato, A., Armigliato, A., Basili, R., Bernardi, F., Brizuela, B., Cerminara, M., de' Micheli Vitturi, M., Di Bucci, D., Di Manna, P., Esposti Ongaro, T., Lacanna, G., Lorito, S., Løvholt, F., Mangione, D., Panunzi, E., Piatanesi, A., 655 Ricciardi, A., Ripepe, M., Romano, F., Santini, M., Scalzo, A., Tonini, R., Volpe, M., and Zaniboni, F.: Tsunami risk management for crustal earthquakes and non-seismic sources in Italy, Riv. Nuovo Cim., 44, 69–144, https://doi.org/10.1007/s40766-021-00016-9, 2021.

Solís, I. and Gazmuri, P.: Evaluation of the risk and the evacuation policy in the case of a tsunami in the city of Iquique, Chile, Natural Hazards, 88, https://doi.org/10.1007/s11069-017-2876-5, 2017.

660 Speranza, F., Pompilio, M., D'Ajello Caracciolo, F., and Sagnotti, L.: Holocene eruptive history of the Stromboli volcano: Constraints from paleomagnetic dating, Journal of Geophysical Research: Solid Earth, 113, https://doi.org/10.1029/2007JB005139, 2008.

Tinti, S., Manucci, A., Pagnoni, G., Armigliato, A., and Zaniboni, F.: The 30 December 2002 landslide-induced tsunamis in Stromboli: sequence of the events reconstructed from the eyewitness accounts, Natural Hazards and Earth System Sciences, 665 5, 763–775, https://doi.org/10.5194/nhess-5-763-2005, 2005.

Tinti, S., Maramai, A., Armigliato, A., Graziani, L., Manucci, A., Pagnoni, G., and Zaniboni, F.: Observations of physical effects from tsunamis of December 30, 2002 at Stromboli volcano, southern Italy, Bull Volcanol, 68, 450–461, https://doi.org/10.1007/s00445-005-0021-x, 2006a.

Tinti, S., Pagnoni, G., and Zaniboni, F.: The landslides and tsunamis of the 30th of December 2002 in Stromboli analysed 670 through numerical simulations, Bull Volcanol, 68, 462–479, https://doi.org/10.1007/s00445-005-0022-9, 2006b.

Tommasi, P., Baldi, P., Chiocci, F. L., Coltelli, M., Marsella, M., Pompilio, M., and Romagnoli, C.: The Landslide Sequence Induced by the 2002 Eruption at Stromboli Volcano, in: Landslides: Risk Analysis and Sustainable Disaster Management, edited by: Sassa, K., Fukuoka, H., Wang, F., and Wang, G., Springer, Berlin, Heidelberg, 251–258, https://doi.org/10.1007/3-540-28680-2_32, 2005.

675 Tulius, J.: Lesson from the Past, Knowledge for the Future: Roles of Human Memories in Earthquake and Tsunami Narratives in Mentawai, Indonesia, Paradigma: Jurnal Kajian Budaya, 10, https://doi.org/10.17510/paradigma.v10i2.396, 2020.

Turchi, A., Di Traglia, F., Gentile, R., Fornaciai, A., Zetti, I., and Fanti, R.: Relative seismic and tsunami risk assessment for Stromboli Island (Italy), International Journal of Disaster Risk Reduction, 76, 103002, https://doi.org/10.1016/j.ijdrr.2022.103002, 2022.